# Unique ocean circulation pathways reshape the Indian Ocean oxygen minimum zone with warming

Sam Ditkovsky[1], Laure Resplandy[2], and Julius Busecke[3]

[1]Program in Atmospheric and Oceanic Sciences, Princeton University, Princeton, NJ, USA
[2]Department of Geosciences and High Meadows Environmental Institute, Princeton University, Princeton, NJ, USA
[3]Lamont-Doherty Earth Observatory, Columbia University, New York, NY, USA

**Correspondence:** Sam Ditkovsky (samjd@princeton.edu)

**Abstract.** The global ocean is losing oxygen with warming. Observations and Earth system model projections suggest, however, that this global ocean deoxygenation does not equate to a simple and systematic expansion of tropical oxygen minimum zones (OMZs). Previous studies have focused on the Pacific Ocean; they showed that the outer OMZ deoxygenates and expands as oxygen supply by advective transport weakens, the OMZ core oxygenates and contracts due to a shift in the composition

5  of the source waters supplied by slow mixing, and in between these two regimes, oxygen is redistributed with little effect on OMZ volume. Here, we examine the OMZ response to warming in the Indian Ocean using an ensemble of Earth system model high-emissions scenario experiments from the Coupled Model Intercomparison Project phase 6. We find a similar expansion-redistribution-contraction response, but show that the unique ocean circulation pathways of the Indian Ocean leads to far more prominent OMZ contraction and redistribution regimes than in the Pacific Ocean. As a result, only the outermost OMZ layers

10  (oxygen $> 180\,\mu\mathrm{mol/kg}$) expand. The Indian Ocean experiences a broad oxygenation in the southwest driven by a reduction in waters supplied by the Indonesian Throughflow in favor of high-oxygen waters supplied from the South Indian Gyre. Models also project a strong localized deoxygenation in the northern Arabian Sea due to the rapid warming and shoaling of marginal sea outflows (Red Sea and Persian Gulf). We extend the existing conceptual framework used to explain the Pacific OMZ response to interpret the response in the Indian Ocean.

15

## 1 Introduction

Oxygen minimum zones (OMZs) are naturally occurring low-oxygen regions located in subsurface tropical oceans (typically 100-1500 m). OMZs develop in the "shadow zones" of the ocean thermocline where oxygen supply by ocean circulation is weak (Luyten et al., 1983; Pedlosky, 1983), and are generally located below highly productive surface systems that boost

20  respiration and biological oxygen demand at the subsurface (Paulmier and Ruiz-Pino, 2009). The global ocean has lost oxygen in response to global warming (Keeling et al., 2010; Helm et al., 2011; Schmidtko et al., 2017; Bindoff et al., 2019), and this trend is expected to continue and accelerate over the twenty-first century if anthropogenic emissions are not significantly drawn

down (Bopp et al., 2013; Kwiatkowski et al., 2020). Global deoxygenation has been attributed to weakening ocean ventilation (i.e., weakening oxygen supply by ocean circulation and mixing) and decreasing oxygen solubility in seawater with warming

25   (e.g., Oschlies et al., 2018). A concern is that OMZs are expanding in response to global deoxygenation, potentially disrupting the physiology and survival of marine organisms and compressing the habitats of marine species requiring oxygen for their survival (Vaquer-Sunyer and Duarte, 2008; Miller et al., 2002; Stramma et al., 2008, 2012; Deutsch et al., 2020; Levin, 2018). The fate of OMZs under warming, in particular the two most intense regions found in the tropical Pacific Ocean and tropical Indian Ocean, has however been highly debated, with apparently inconsistent changes found across hydrographic observations,

30   paleo-oceanographic proxies and Earth system model (ESM) projections. In-situ hydrographic observations collected since the 1950s suggest that the tropical Indo-Pacific Oceans and the marginal seas that supply oxygen to the tropical Indian Ocean (including the Persian Gulf and Red Sea) have lost oxygen, supporting the view that tropical OMZs are expanding (Stramma et al., 2008; Helm et al., 2011; Ito et al., 2017; Banse et al., 2014; Piontkovski and Al-Oufi, 2015; Queste et al., 2018; Naqvi, 2021). Yet, paleo-oceanographic studies suggest that the OMZ in the eastern tropical Pacific Ocean has contracted, rather than

35   expanded, under past warming conditions (Deutsch et al., 2014; Auderset et al., 2022). Looking into the future, studies using ESM ensembles have projected a robust deoxygenation at mid- and high-latitudes with warming, consistent with the weakening of ventilation found at the global scale, but have failed, until recently, to reach a consensus on the expected changes in oxygen and OMZ volumes in tropical oceans (Cocco et al., 2013; Bopp et al., 2013; Cabré et al., 2015; Bopp et al., 2017; Resplandy, 2018; Kwiatkowski et al., 2020).

40   Busecke et al. (2022) recently showed that the inconsistencies found in the fate of the OMZ in the Pacific Ocean could be reconciled using an ensemble of ESMs from the Coupled Model Intercomparison Project Phase 6 (CMIP6; Eyring et al., 2016). They found that the OMZ response to global warming was in fact consistent across the ESMs when examined in an oxygen-space framework and fell into three regimes: an expansion of the OMZ outer layers (large OMZ volume delimited by oxygen thresholds of typically $\sim 100\,\mu\mathrm{mol/kg}$ or higher), a contraction of the eastern Pacific "OMZ core" waters (OMZ volume

45   delimited by oxygen thresholds of $\sim 20\,\mu\mathrm{mol/kg}$ or lower), and a "transition regime" between contraction and expansion that experiences weak and uncertain changes associated with a spatial redistribution of the OMZ volume. This three-regime framework reconciles hydrographic work that show an OMZ expansion in the central Pacific Ocean where the OMZ outer layers are located (Stramma et al., 2008), and paleo-oceanographic studies that found evidence for a contraction in the eastern Pacific (note that these studies used nitrogen isotopes which are a proxy for "OMZ core" denitrifying waters; Deutsch et al., 2014;

50   Auderset et al., 2022). The framework also explains the discrepancies found in previous modeling studies that often considered OMZ volume definitions that fall in the transition regime where changes are smaller and uncertain (e.g., Bopp et al., 2013; Cabré et al., 2015). In the Pacific Ocean, the apparent discrepancy between outer OMZ expansion and core contraction can be interpreted using the conceptual framework proposed by Gnanadesikan et al. (2007), which distinguishes between two models of ocean ventilation: (1) a "single-pipe" model where ventilation is controlled by advection from one source water mass, and

55   (2) a "mixing-network" model in which ventilation rates are sustained by slow mixing of multiple source waters as in ocean shadow zones (Lévy et al., 2022; Gnanadesikan et al., 2013; Brandt et al., 2015). As ocean circulation pathways weaken, regions ventilated by a single-pipe experience reduced supply of oxygen (transport rates of oxygenated surface water to the

thermocline slows), while regions ventilated by a mixing-network can either experience a reduction or increase in ventilation and oxygen supply (by changing the connectivity and the contributions of each source water to the mixing-network). The single-pipe model explains the deoxygenation of the outer OMZ layers, which has been attributed to the weakening of the northern and southern subtropical cells that ventilate the outer layers of the OMZ (Gnanadesikan et al., 2012; Duteil et al., 2014; Busecke et al., 2022; Duteil et al., 2021; Llanillo et al., 2018; Margolskee et al., 2019). In contrast, changes in mixing-network connectivity explain the oxygenation of the Pacific OMZ core, which was attributed to reduced contributions from aged, oxygen-poor deep and intermediate waters, shifting the mixing ratio towards younger, oxygen-rich upper ocean waters (Bryan et al., 2006; Gnanadesikan et al., 2007, 2012; Takano et al., 2018; Busecke et al., 2022).

The fate of the Indian Ocean OMZ has been far less studied than its Pacific Ocean counterpart. Yet, the Indian Ocean shows some of the fastest ocean warming trends in the world (Roxy et al., 2014; Sharma et al., 2023), and the expansion of its OMZ could have detrimental effects for coastal populations that depend heavily on marine resources for food security and economic stability in the region (Bouchard and Crumplin, 2010; Clifton et al., 2012; Gattuso et al., 2015; Llewellyn et al., 2016; Roy, 2019). The ventilation pathways and OMZ geometry in the Indian Ocean are fundamentally different from the two subtropical cells (one in each hemisphere) and eastern boundary OMZ found in the Pacific Ocean. It is thus unclear whether the "single-pipe and mixing-network" framework which characterizes the Pacific Ocean is sufficient to describe the behavior of the Indian Ocean. The Indian Ocean is bounded by continent to the north and ventilation is almost exclusively sustained by one subtropical cell originating in the South Indian Gyre (Harper, 2000; Schott et al., 2002; Phillips et al., 2021). As a result, oxygen levels are higher in the southern Indian Ocean while an OMZ extends over most of the Arabian Sea and the Bay of Bengal in the north (see Figure 1 for observed climatological oxygen field and major ventilation pathways). Other peculiarities of the Indian Ocean ventilation are the Indonesian Throughflow which brings waters from the tropical Pacific Ocean into the Southern Indian Ocean (Sprintall et al., 2009), and the saline marginal sea outflow waters from the Red Sea and Persian Gulf that ventilate the Arabian Sea (Rhein et al., 1997; Beal et al., 2000; Menezes, 2021; Sheehan et al., 2020). Ventilation by all these advective pathways (Southern Gyre, Indonesian Throughflow and marginal seas) is projected to weaken in response to climate change (Sen Gupta et al., 2016; Feng et al., 2017; Stellema et al., 2019; Lachkar et al., 2019; Kobayashi et al., 2012), but the extent to which these changes in ventilation will affect basin-scale oxygen content and the OMZ in the Indian Ocean is however still poorly constrained. Here, we examine changes in oxygen content and OMZ volume in the Indian Ocean in response to climate change using an ensemble of CMIP6-generation ESMs with a focus on thermocline depths (upper 1000 m). We show that the fate of the Indian Ocean OMZ is consistent with the three-regime framework identified in the Pacific Ocean (Busecke et al., 2022) but that broad oxygenation results in a much more prominent contraction regime in the Indian Ocean than in the Pacific Ocean. Interpreting these changes in oxygen and OMZ volume in the Indian Ocean calls for an extension of the single-pipe and mixing-network conceptual framework to include the unique contributions from the Indonesian Throughflow and marginal seas, which we show can be interpreted as "two-pipe" and "moving-pipe" systems.

## 2   Methods

### 2.1   Datasets

We use an ensemble of 8 ESMs from the CMIP6 archive (Eyring et al., 2016; O'Neill et al., 2016). Out of the 14 CMIP6 ESMs that provided monthly dissolved oxygen data for the pre-industrial control, historical, and SSP5-8.5 experiments (Busecke et al., 2022), 5 models do not simulate an OMZ core in the Arabian Sea (ACCESS-ESM1-5, CanESM5, CanESM5-CanOE, IPSL-CM6A-LR; Fig S1), and 1 additional model has an extraordinary bias in the low oxygenated waters (CNRM-ESM2-1; Fig S2), simulating nearly double the observed volume of waters below $150 \, \mu\mathrm{mol/kg}$ in the Indian Ocean. We keep the 8 remaining ESMs (GFDL-CM4, GFDL-ESM4, MIROC-ES2L, MPI-ESM1-2-HR, MPI-ESM1-2-LR, NorESM2-LM, NorESM2-MM, UKESM1-0-LL). Indeed, ESMs tend to overestimate oxygen concentrations in the Arabian Sea (Oschlies et al., 2008; Bopp et al., 2013; Rixen et al., 2020). A common source of this bias is unrealistically strong ventilation from the Red Sea Outflow, where the narrow outflow channel is difficult to represent on a coarse ocean grid, which results in elevated oxygen levels in the Arabian Sea (Schmidt et al., 2021). We find that 3 out of the 5 discarded ESMs with particularly high oxygen concentrations in the Arabian Sea (CanESM5, CanESM5-CanOE and IPSL-CM6A-LR) are characterized by annual average Red Sea outflow rate more than double the observed rate (Fig. S3; Sofianos and Johns, 2007). For this analysis, we use oxygen, salinity, potential temperature and when available, ideal age and mass transport (7 ESMs have ideal age and 5 have mass transport). Only one member is used for each model. See Table 1 for member labels and data availability of each model. All model outputs were regridded to a uniform $1° \times 1°$ grid using the xESMF python package (Zhuang et al., 2021), but transport calculations were performed on each model's native grid (Sect. 2.2.3). The pre-industrial simulations were used to remove the linear control drifts from all scalar fields (oxygen, salinity, temperature, ideal age) in the historical and SSP5-8.5 simulations using the xMIP python package to unify metadata between parent and child simulations (Busecke and Spring, 2020).

We also use the observational climatology of dissolved oxygen concentrations from the World Ocean Atlas 2018 (WOA18; Garcia et al., 2019) to evaluate the representation of the Indian Ocean OMZ and dissolved oxygen field in the ensemble of ESMs. We use an average over the period of 1950-2015 in the historical simulations to compare to the observed climatology.

### 2.2   Analysis

To characterize the response of ocean variables to climate change, we used linear trends over the 2015-2100 period in the SSP5-8.5 simulations (normalized to change per century), except when calculating water mass mixing ratios (Sect. 2.2.4), for which we compare historical (1950-2015 average) and end-of-century (historical plus 75-year trend) states. To represent the ESM ensemble, we take the mean over models (multi-model mean) and use one standard deviation of the model spread as a measure of uncertainty. When presenting multi-model mean trend fields, we stipple where less than 75% of available models agree on the sign of change to indicate regions of uncertainty. While we perform our analysis over the full water column, we focus on thermocline depths (upper 1000 m) so that the results may characterize impacts on mesopelagic ecosystems. When examining oxygen and ideal age trends, we exclude surface waters by examining changes between 100 and 1000 m.

**Table 1.** ESM data used in this study. Variables used: Dissolved oxygen concentration (o2), salinity (so), potential temperature (thetao), ideal age (agessc) and mass transport (umo/vmo) where available. All data used in this study is publically available via ESGF, except ideal age fields from GFDL-CM4 and GFDL-ESM4 (see Busecke et al., 2022)

| ESM | Variables | Member ID |
|---|---|---|
| GFDL-CM4 (Guo et al., 2018a, b) | o2, thetao, so, agessc | r1i1p1f1 |
| GFDL-ESM4 (Krasting et al., 2018; John et al., 2018) | o2, thetao, so, agessc | r1i1p1f1 |
| MIROC-ES2L (Hajima et al., 2019; Tachiiri et al., 2019) | o2, thetao, so, agessc | r1i1p1f2 |
| MPI-ESM1-2-HR (Jungclaus et al., 2019; Schupfner et al., 2019) | o2, thetao, so, agessc, umo/vmo | r1i1p1f1 |
| MPI-ESM1-2-LR (Wieners et al., 2019b, a) | o2, thetao, so, agessc, umo/vmo | r1i1p1f1 |
| NorESM2-LM (Seland et al., 2019a, b) | o2, thetao, so, agessc, umo/vmo | r1i1p1f1 |
| NorESM2-MM (Bentsen et al., 2019a, b) | o2, thetao, so, agessc, umo/vmo | r1i1p1f1 |
| UKESM1-0-LL (Tang et al., 2019; Good et al., 2019) | o2, thetao, so, umo/vmo | r1i1p1f2 |

### 2.2.1 Tracking ocean volume by oxygen threshold

OMZ volume is generally defined as the volume of water below a chosen oxygen concentration threshold. We extend this idea to a wide range of oceanic oxygen concentration values. Here, we define the full column OMZ volume as a function of oxygen thresholds, $O_{2,T}$ (following Busecke et al., 2022):

$$\mathcal{V}_{O_2}(O_{2,T}) = \iiint_{O_2 \leq O_{2,T}} dV \tag{1}$$

where we integrate over the Indian Ocean from $30°\,S$ - $25°\,N$ and from the African continent to the west to Indonesia and Australia, extending to about $125°\,E$ in the main strait of the Indonesian Throughflow, to the east. The Red Sea and Persian Gulf are not included in the integration of $\mathcal{V}_{O_2}$. However, we do not focus on the full OMZ volume, but rather the thermocline OMZ volume:

$$\mathcal{V}_{O_2^{1000}}(O_{2,T}) = \int_0^{1000m} \iint_{O_2 \leq O_{2,T}} dV \tag{2}$$

Note that we integrate over the upper 1000 m here, rather than 100 to 1000 m, because OMZ volume will naturally exclude surface waters. In both cases, we use oxygen thresholds $O_{2,T}$ that vary between 5 and $225\,\mu\text{mol/kg}$ and highlight two benchmark thresholds: (1) $O_{2,T} = 60\,\mu\text{mol/kg}$ (OMZ60) as a commonly cited threshold for hypoxia at which marine ecosystems tend to experience significant loss of biodiversity (Vaquer-Sunyer and Duarte, 2008), and (2) $O_{2,T} = 150\,\mu\text{mol/kg}$ (OMZ150) as a common habitat boundary for large commercial fish species such as tuna (Brill, 1996; Prince and Goodyear, 2006; Bertrand et al., 2011; Stramma et al., 2012; Dueri et al., 2014). We also discuss changes in the OMZ core ($O_{2,T} = 20\,\mu\text{mol/kg}$) as used in (Busecke et al., 2022).

### 2.2.2 Thermal and non-thermal dissolved oxygen trends

140 We separate the influences of thermal and non-thermal processes on oxygen trends. The thermal component, or oxygen saturation $O_{2SAT}$, is calculated using the `GSW-python` package from potential temperature and salinity fields (Firing et al., 2021). The non-thermal component, related to ocean ventilation and biological sources and sinks of oxygen, is computed as the residual between $O_2$ and $O_{2SAT}$ and is referred to as Apparent Oxygen Utilization (AOU):

$$O_2 = O_{2SAT} - AOU \tag{3}$$

145 We compute $O_{2SAT}$ and AOU for each year in the historical and SSP5-8.5 simulations, then take historical means and projected linear trends. Trends in $-AOU$ represent the contribution of non-thermal processes to overall changes in dissolved oxygen but they encompass both changes in physical (ventilation changes tied to slower circulation or changes in mixing) and biological (respiration rates) effects. We use the ideal age of seawater (i.e., the time since exposure to the surface) to qualitatively infer the contribution of physical ventilation changes, and compute the Pearson Correlation Coefficients between interannual anoma-

150 lies in ideal age and AOU over the SSP5-8.5 experiment (calculated with respect to a 1950-2015 mean from the historical simulations) to assess the importance of ventilation changes compared to biological changes.

### 2.2.3 Quantifying changes in transport by ventilation pathways

To help interpret trends in dissolved oxygen and ideal age, we quantify changes in individual thermocline ventilation pathways using mass transport fields on each model's native grid. The Indonesian Throughflow Water transport is calculated as the

155 westward flow through the main strait of the Indonesian Throughflow (the Timor Sea) integrated between 100 and 1000 m. The Southern Pathway Waters transport is calculated as the northward flow across 30°S integrated between 100 and 1000 m. The upwelling of Deep Waters into the thermocline is calculated as the budget residual of transport below 1000 m across 30°S and through the main strait of the Indonesian Throughflow. Transports by marginal sea outflows from the Red Sea and Persian Gulf are defined as the outflowing components through their respective channels. We report transport trends in Sv/century,

160 using a constant reference density of $1025 \, \text{kg/m}^3$ to convert between mass and volume transport. Transport fields are available for 5/8 ESMs in the ensemble (MPI-ESM1-2-HR, MPI-ESM1-2-LR, NorESM2-LM, NorESM2-MM, UKESM1-0-LL).

### 2.2.4 Identifying changes in water mass mixing ratios

In sections 3.5 and 3.6, we solve a mixing model in the South Equatorial Current and in the Arabian Sea to evaluate shifts in water mass mixing ratios under SSP5-8.5 forcing. The mixing model is based on extended Optimum Multiparameter Analysis

165 (OMP) (Tomczak and Large, 1989; Karstensen and Tomczak, 1998). This technique solves for the mixing ratios at a given hydrographic section using the hydrographic properties of specified source water masses (see references and Appendix A for details). We use a python implementation (`pyOMPA` Shrikumar et al., 2022), based on the original MATLAB code from Karstensen and Tomczak (1998). We perform this analysis along potential density surfaces referenced to zero pressure ($\sigma_0$), calculated from potential temperature and salinity fields using the `GSW-python` package (Firing et al., 2021). For each region,

170  we use a nominal value for potential density that captures features of significant dissolved oxygen change; however, we tune this value slightly (within 0.5) for individual ESMs to better capture features across models.

The number of source water masses is limited to be less than or equal to the number of hydrographic properties available. Here, we use potential temperature, salinity, dissolved oxygen and AOU. To account for remineralization along the pathways (between source and case study regions), we allow for the conversion of dissolved oxygen to AOU (see Appendix A for details).

175  In the case of the South Equatorial Current region, the source waters are Indonesian Throughflow Water, Southern Pathway Waters and Arabian Sea Water, determined at $(15°\,S, 120°\,E)$, $(30°\,S, 100°\,E)$ and $(15°\,N, 65°\,E)$ respectively at a nominal potential density of $\sigma_0 = 26.4$. In the case of the Arabian Sea, the source waters are Persian Gulf Water, Red Sea Outflow Water and Arabian Sea Water determined at $(24.5°\,N, 58.5°\,E)$, $(12°\,N, 47°\,E)$ and $(15°\,N, 65°\,E)$ respectively at a nominal potential density of $\sigma_0 = 25.7$.

180  For each ESM in the ensemble, we solve this mixing model for a historical state and an end-of-century state. For the historical state, we first compute potential density for the historical mean (1950-2015) for each ESM, and use the `xgcm` (Nicholas et al., 2023) package to transform the vertical coordinates of each model to potential density space. We note that the results of the mixing model are not sensitive to the order of operations (temporal averaging and vertical transformation). To compute an end-of-century state, we add 75-year (2015-2100) forced trends from the SSP5-8.5 simulations to historical

185  mean fields (potential temperature, salinity, oxygen, AOU) to represent a climatological year 2100, then repeat the coordinate transformation described above.

A concern when solving for forced trends on a potential density layer is that the results may be influenced by the displacement of this isopycnal in depth. Indeed, the potential density layers chosen here are displaced deeper in the water column by about 100 m between the historical and end-of-century states. To evaluate the impact of this deepening, we perform an alternate set

190  of mixing model experiments where we use a lower density value to evaluate the end-of-century state than used to evaluate the historical state. This lower density value is tuned to sample the same depth as was sampled for the historical state. The results of this alternative analysis, presented in Supplementary Information, are qualitatively similar to the analysis presented in the main text, and do not change the main results.

## 3  Results

195  ### 3.1  Historical oxygen and ventilation pathways in observations and Earth system models

The observed oxygen distribution in the Indian Ocean thermocline (100 to 1000 m) is influenced by five main ventilation pathways (Fig. 1a-c). First, the Southern Pathway Waters which enter via the South Indian Gyre include (from least to most dense) Subtropical Underwater (STUW; about 100 to 250 m depth), Indian Central Water and Subantarctic Mode Water (CW+MW; about 250 to 750 m depth) and Antarctic Intermediate Water (IW; about 750 to 1000 m depth) (Sprintall and Tomczak, 1993;

200  Karstensen and Tomczak, 1997; McCarthy and Talley, 1999; Karstensen and Quadfasel, 2002; Fine, 1993; Talley, 2011). This spectrum of waters enters the basin with a range of oxygen between about 160 to $250\,\mu\mathrm{mol/kg}$, where Indian Central Water and Subantarctic Mode Water account for the highest oxygen levels. Southern Pathway Waters are capped by the salinity max-
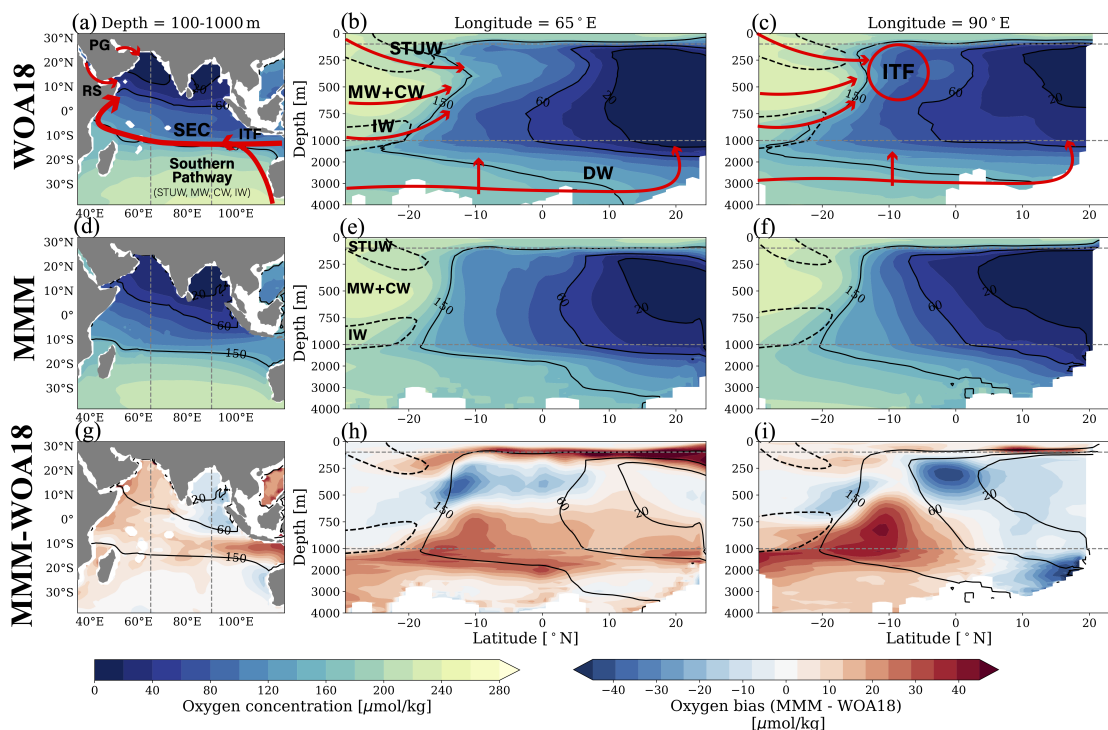
**Figure 1.** Dissolved oxygen annual mean climatology from World Ocean Atlas 2018 (WOA18) **(a)** averaged between 100 and 1000 m, at **(b)** 65°E and **(c)** 90°E. Multi-model mean (MMM) dissolved oxygen in the Indian Ocean for historical period (1950-2015) **(d)** between 100 and 1000 m, **(e)** at 65°E, and **(f)** at 90°E. Difference between MMM (1950-2015) and WOA18 dissolved oxygen **(g)** between 100 and 1000 m, **(h)** at 65°E, and **(i)** at 90°E. Solid black contours represent 20, 60 and 150 μmol/kg oxygen in **(a-c)** WOA18 and **(d-i)** MMM. **(a,d,g)** Dashed gray lines indicate 65°E and 90°E. **(b,c,e,f,h,i)** Dashed gray lines indicate depth of 100 and 1000 m, dashed black contours show salinity contours highlighting Subtropical Underwater and Intermediate Water. Water masses and ventilation pathways are illustrated schematically. Abrevations: South Equatorial Current (SEC), Central Water (CW), Deep Water (DW), Subtropical Underwater (STUW), Mode Water (MW), Intermediate Water (IW), Indonesian Throughflow (ITF).

imum of Subtropical Underwater and the salinity minimum of Antarctic Intermediate Water (dashed black contours in Fig. 1b,c) Second, the Indonesian Throughflow (ITF) brings waters from the tropical Pacific Ocean (with oxygen concentrations of

205    about 80-170 μmol/kg between 100 to 1000 m depth) into the Southern Indian Ocean and which mix with Southern Pathway Waters in the South Equatorial Current (SEC). This mixture of waters then crosses the equator with the western boundary current to ventilate the northern basin (pathway schematic in Fig. 1a) via eddy mixing, monsoonal currents and the weak North Equatorial Current which flows east in the summer along about 5°N (Schott et al., 2009; Phillips et al., 2021; Resplandy et al., 2012; Lachkar et al., 2016). In the northern Indian Ocean, two additional pathways are associated with saline marginal sea

210    outflows: Red Sea Outflow Water (RS, with concentrations around 70 μmol/kg) and Persian Gulf Water (PG, near oxygen saturation >200 μmol/kg) deliver oxygen directly to the OMZ core in the Arabian Sea as they are are quickly diluted by mix-
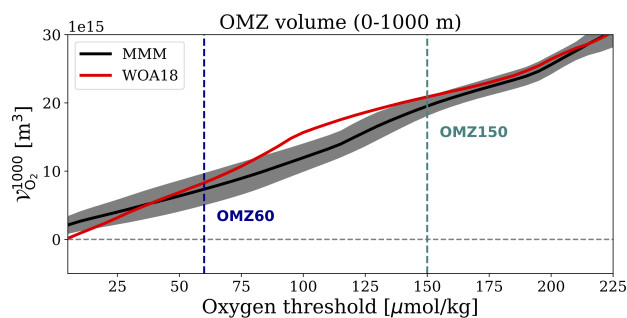
**Figure 2.** OMZ volume taken between 0-1000 m in the Indian Ocean for the multi-model mean averaged over 1950-2015 (MMM; black) and observed climatology (WOA18; red). Shading represents one standard deviation of the model spread.

ing (Fig. 1a). Finally, the fifth pathway corresponds to Deep Waters (DW) that enter from the Southern Ocean and Indonesian Throughflow (here taken as waters below 1000 m depth) and slowly upwell in the basin (McCarthy et al., 1997), ventilating the thermocline from below with relatively well oxygenated waters (100 - 200 $\mu$mol/kg).

215   The multi-model mean (eight ESMs, see methods) captures the main features associated with the five pathways ventilating the Indian Ocean (Fig. 1d-f). In particular, the oxygen supply by the Southern Pathway and the Indonesian Throughflow is relatively well simulated (Fig. 1a-c), with an oxygen maximum associated with Indian Central Water and Subantarctic Mode Water. The multi-model mean simulates the full spectrum of Southern Pathways Waters, indicated by the salinity maximum and minimum associated with Subtropical Underwater and Antarctic Intermediate Water (dashed black contours in Figure 1e,f),

220   and overall captures the temperature and salinity properties of water masses across the basin (Fig. S4). Overall, the simulated thermocline ventilation pathways maintain a realistic meridional oxygen gradient with well oxygenated waters in the southern basin and OMZ cores in the Arabian Sea and Bay of Bengal (contours of 20, 60 and 150 $\mu$mol/kg water extent shown in solid black contours in Fig. 1). There are, however, several regions of bias in the simulated oxygen field (Fig. 1g-i). For example, the multi-model mean simulates higher than observed oxygen levels in the subsurface Arabian Sea (Fig. 1h). This is a well

225   documented bias among ESMs (Oschlies et al., 2008; Bopp et al., 2013; Rixen et al., 2020; Schmidt et al., 2021) that we significantly mitigated in our ensemble by removing models that lacked an OMZ core in the Arabian Sea (Sect. 2.1; Fig. S5).

Despite some biases in the multi-model mean oxygen field, we find good agreement with observed OMZ volumes. We compare thermocline OMZ volume, $\mathcal{V}_{O_2^{1000}}$ (i.e., volume in the upper 1000 m), in observations and the multi-model mean for oxygen thresholds between 5 and 225 $\mu$mol/kg (Fig. 2). In the observed climatology, $\mathcal{V}_{O_2^{1000}}$ increases about linearly with

230   oxygen threshold, with an hypoxic volume OMZ60 of about $8.3\times10^{15}$m$^3$ and an OMZ150 volume of about $21\times10^{15}$m$^3$. The multi-model mean simulates this linear relationship and agrees with observations within 12% for OMZ60 volume and 7% for OMZ150 volume, and at both benchmarks the observations fall within the ensemble spread. For the OMZ core (<20 $\mu$mol/kg), the multi-model mean overestimates observed volumes by about 50%
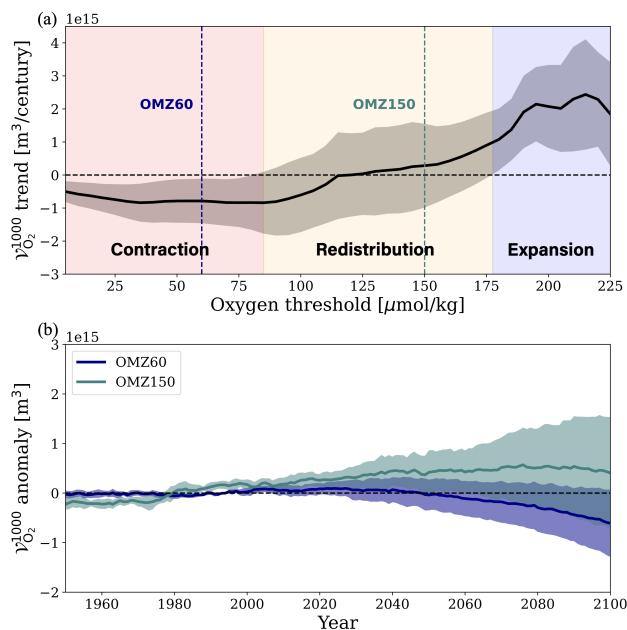
9

**Figure 3.** Multi-model mean thermocline OMZ volume changes (between 0 - 1000 m) under SSP5-8.5 scenario forcing (2015-2100). **(a)** $\mathcal{V}_{O_2^{1000}}$ trends as a function of oxygen threshold. The 60 and 150 $\mu$mol/kg thresholds bounding OMZ60 and OMZ150 are indicated with dark blue and teal dashed lines. **(b)** Time series of $\mathcal{V}_{O_2^{1000}}$ anomaly from 1950-2100 (anomaly referenced to 1950-2015 mean) for OMZ60 (dark blue) and OMZ150 (teal). Shading represents one standard deviation of model spread.

### 3.2 Projected OMZ volume exhibits diverging trends at low and high oxygen thresholds

235     Projections of thermocline OMZ volume under SSP5-8.5 forcing fall into three regimes: a robust expansion of OMZ volumes set by high oxygen thresholds (above 180 $\mu$mol/kg), a robust contraction of volumes set by low oxygen thresholds (below 85 $\mu$mol/kg), and a transition regime with weak and uncertain trends characterized by redistribution of OMZ volume (between 85 and 180 $\mu$mol/kg; Fig. 3a). We define robust OMZ expansion and contraction as where the multi-model mean trends exceed one standard deviation of the model spread. The volume of hypoxic waters, OMZ60, contracts at a rate

240     of $0.8\pm0.7\times10^{15}$m$^3$/century, with the multi-model mean signal emerging from the model spread only at the end of the twenty-first century (Fig. 3b). This signal is similar for the OMZ core ($<20\,\mu$mol/kg), where the multi-model mean projects a contraction rate of $0.7\pm0.4\times10^{15}$m$^3$/century. Meanwhile, the OMZ150 falls between the regimes of robust expansion and contraction and experiences near-zero volume trends in the multi-model mean. Tracking the evolution of the OMZ150, we see that ESMs project an expansion over the first half of the twenty-first century before disagreeing on the trajectory in the latter

245     half of the century (Fig. 3b). By 2100, four ESMs project an expansion of the OMZ150 and four project a contraction.
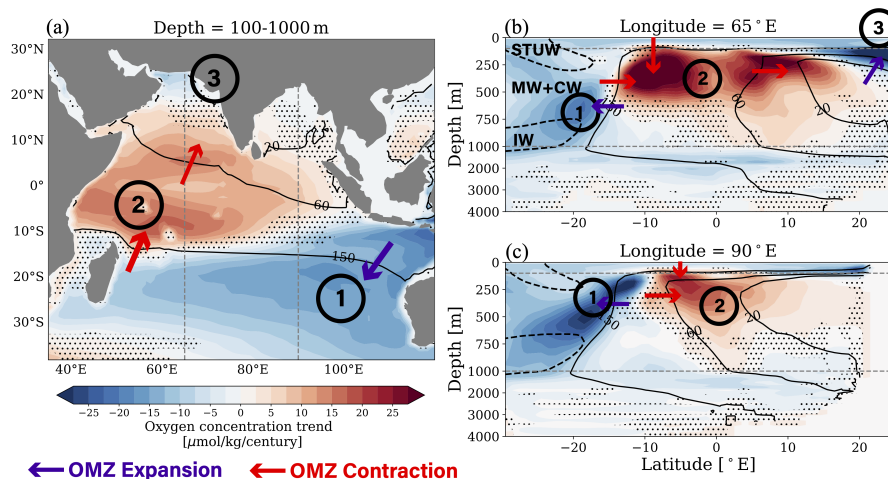
**Figure 4.** Multi-model mean (MMM) dissolved oxygen trends under SSP5-8.5 scenario forcing (1915-2100). Dissolved oxygen trends **(a)** bewtween 100 and 1000 m, **(b)** at 65°E and **(c)** at 90°E. Dashed gray lines mark **(a)** 65°E and 90°E, and **(b,c)** 100 and 1000 m. **(b,c)** Solid black contours represent 20, 60 and 150 $\mu$mol/kg oxygen. Dashed black contours highlight salinity signatures of Subtropical Underwater (STUW) and Intermediate Water (IW), with Central Water (CW) and Mode Water (MW) between. Main features of dissolved oxygen trends numbered, with effect on OMZ volume indicated by purple and red arrows. Results are stippled where less than 75% (6/8) of models agree on sign of trend.

### 3.3 Regional contrasts in dissolved oxygen trends reshape the Indian Ocean OMZ

Projected trends in dissolved oxygen are highly variable in space, both horizontally and vertically, leading to regional contraction, expansion and redistribution of the OMZ volume (Fig. 4). The multi-model mean projects a weak increase in oxygen in the OMZ cores of the Arabian Sea and Bay of Bengal and a decline in oxygen in the relatively well oxygenated water masses entering via the Southern Pathway and ventilating the OMZ outer layers (Fig. 4). Strongest oxygen changes are, however, found at intermediate oxygen levels, between the core and the outer layers. We focus on the three major features that influence the OMZ volume at these intermediate levels (labeled by numbers in Fig. 4): the deoxygenation in the southeastern basin (Feature 1), the oxygenation of the western South Equatorial Current (Feature 2), and the deoxygenation in the northern Arabian Sea (Feature 3). All three features of dissolved oxygen trends are captured in all individual ESMs in the ensemble (Fig. S6,S7), leading to a robust pattern in the multi-model mean (more than 75% of models agree on sign of trend; Fig. 4). Feature 1 coincides with the flow of Southern Pathway Waters in the subtropical gyre and Indonesian Throughflow Water entering the Indian Ocean. Indeed, we see two distinct maxima of the deoxygenation along the meridional section at 90°E (Fig. 4c): one coinciding with Southern Pathway waters (namely Central, Mode and Intermediate Waters) centered around 500 m depth with deoxygenation rates up to 35 $\mu$mol/kg/century, and one coinciding with Indonesian Throughflow waters at around 250 m depth with deoxygenation rates up to 50 $\mu$mol/kg/century. Feature 2 is located where Southern Pathway Waters and Indonesian Throughflow waters mix within the South Equatorial Current. Feature 2 has a maximum oxygenation trend in the South Equatorial Current
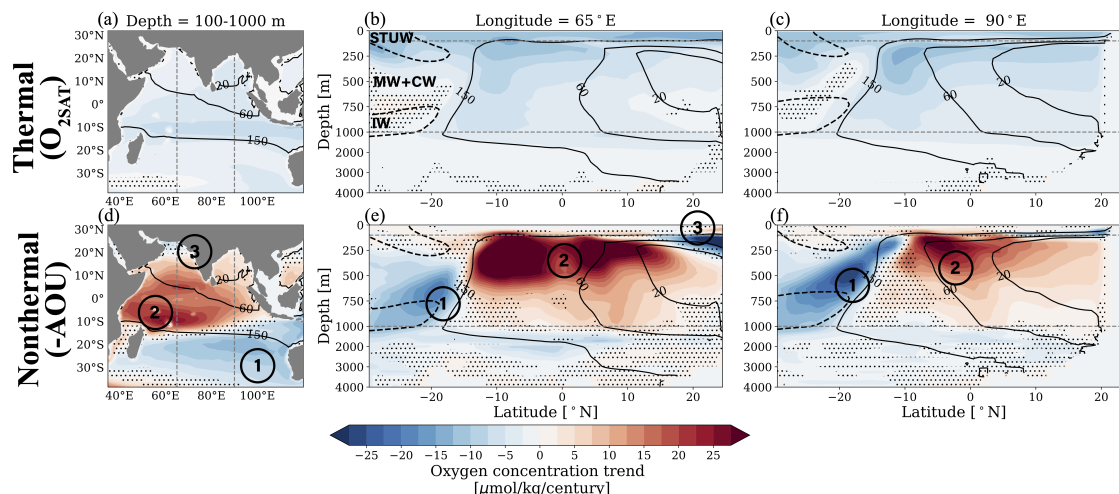
**Figure 5.** Thermal and non-thermal components of multi-model mean (MMM) dissolved oxygen trends under SSP5-8.5 scenario forcing (1915-2100). Thermal oxygen ($O_{2SAT}$) trends **(a)** between 100 and 1000 m, **(b)** at 65°E and **(c)** at 90°E. Non-thermal oxygen (-AOU) trends **(d)** between 100 and 1000 m, **(e)** at 65°E and **(f)** at 90°E. Dashed gray lines mark **(a,d)** 65°E and 90°E, and **(b,c,e,f)** 100 and 1000 m. **(b,c,e,f)** Solid black contours represent 20, 60 and 150 $\mu$mol/kg oxygen. Dashed black contours represent salinity contours highlighting Subtropical Underwater (STUW) and Intermediate Water (IW), with Central Water (CW) and Mode Water (MW) between. Main features of dissolved oxygen trends numbered. Results are stippled where less than 75% (6/8) of models agree on sign of trend.

between 100 and 500 m, where waters oxygenate at a rate of up to about 50 $\mu$mol/kg/century, and a secondary maximum in the North Equatorial Current, with oxygenation rates up to 40 $\mu$mol/kg/century (Fig. 4a-b). Together, Features 1 and 2 form an oxygenation dipole along the path of the South Equatorial Current. Lastly, Feature 3 is a deoxygenation in the northern
265 Arabian Sea between about 100 and 300 m depth where the Persian Gulf Outflow dominates ventilation (Fig. 4a-b). Waters in Feature 3 deoxygenate at a rate of up to about 60 $\mu$mol/kg/century.

These three features ultimately explain the contraction, expansion, and redistribution of the OMZ volume at thermocline depths across oxygen thresholds. The deoxygenation of in the southeastern basin (Feature 1) is the primary driver of OMZ expansion at high oxygen thresholds (expansion regime, Fig. 3b). The oxygenation dipole (from Features 1 and 2) redistribute
270 the OMZ volume from west to east and explains the weak volume changes found at intermediate oxygen thresholds including the volume of the OMZ150 (redistribution regime, Fig. 3b). The oxygenation in the South Equatorial Current, and in turn the western boundary current waters (Feature 2), contributes to the OMZ contraction at low oxygen thresholds including the volume of OMZ60 (contraction regime, Fig. 3b), although the net change in volume is relatively small due to the compensating expansion in the northern Arabian Sea which also affects the low oxygen thresholds (Feature 3).
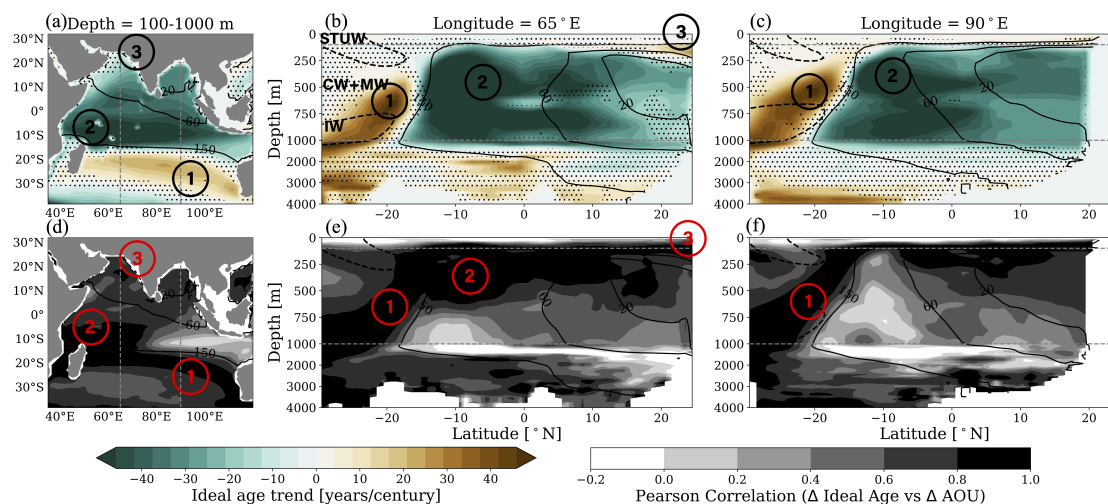
**Figure 6.** Multi-model mean (MMM) ideal age trends under SSP5-8.5 scenario forcing (2015-2100) **(a)** between 100 and 1000 m, **(b)** at 65°E and **(c)** at 90°E. Stippling where less than 75% (6/7) of models agree on sign of trend. Pearson correlation coefficient between anomalies (with respect to 1950-2015 mean) in ideal age and non-thermal changes (AOU) **(d)** between 100 and 1000 m, **(e)** at 65°E and **(f)** at 90°E. Dashed gray lines mark **(a,d)** 65°E and 90°E, and **(b,c,e,f)** 100 and 1000 m. **(b,c,e,f)** Solid black contours represent 20, 60 and 150 $\mu$mol/kg oxygen. Dashed black contours represent salinity contours highlighting Subtropical Underwater (STUW) and Intermediate Water (IW), with Central Water (CW) and Mode Water (MW) between. Main features of dissolved oxygen trends numbered.

## 3.4 Dissolved oxygen trends are dominated by changes in ventilation

To identify which processes control projected dissolved oxygen trends, and in turn the reshaping of the Indian Ocean OMZ, we separate dissolved oxygen trends into thermal and non-thermal components (Fig. 5). Thermal oxygen trends relate to changes in oxygen saturation concentrations, while non-thermal oxygen trends arise from changes in physical ocean circulation and biological respiration rates (Sect. 2.2.2). Thermal and non-thermal effects tend to influence different water masses: thermal trends are strongest in surface waters (above 100 m), while non-thermal trends are strongest at thermocline depths (100 to 1000 m), but are also responsible for deoxygenation in the deep ocean (below 1000 m) (Fig. 5). Thermal oxygen changes drive relatively uniform deoxygenation in the surface ocean of about 5 to 15 $\mu$mol/kg/century. Thermal effects are only significant below 100 m along the pathways of Subtropical Underwater (Fig. 5b) and Indonesian Throughflow Water (Fig. 5a,c). The non-thermal component largely explains the strong patterns of oxygenation and deoxygenation discussed above, including deoxygenation in the southeast, oxygenation in the SEC, and deoxygenation in the northern Arabian Sea (Features 1 to 3; Fig. 4 and 5d-f).

The ideal age of seawater, or the average time since water has been exposed to the surface, is a direct measure of ventilation timescale; trends in ideal age thus indicate changes in the rate of ventilation from advection and mixing. Trends in ideal age agree with the pattern of non-thermal oxygen trends. The regions of maximum decreased ventilation (i.e., waters get
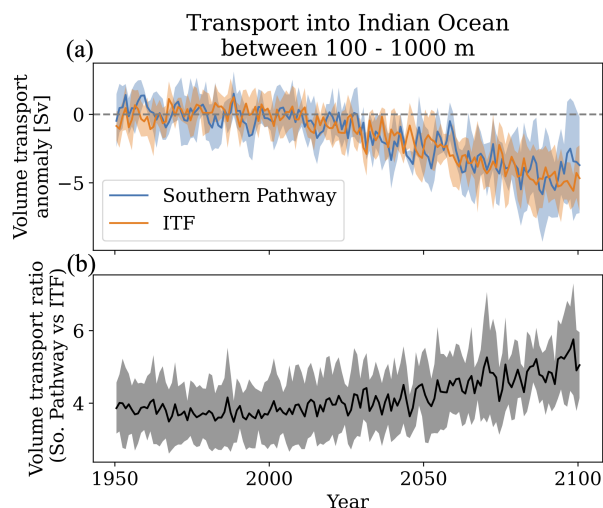
13

**Figure 7. (a)** Interannual transport anomalies (referenced to 1950-2015 mean) for inflowing components of Southern Pathway Waters (blue) and Indonesian Throughflow Water (orange) between 100 and 1000 m. **(b)** Ratio of total inflowing transport of Southern Pathway and Indonesian Throughflow Waters. Solid curves represent multi-model mean (MMM) and shading represents one standard deviation of model spread. Transport data is available for 5 ESMs.

290  older) correspond spatially with deoxygenation in the southeastern basin (Feature 1) and Arabian Sea (Feature 3), while the region of maximum increased ventilation (i.e., waters get younger) corresponds to the region of oxygenation in the South Equatorial Current (Feature 2; Fig. 6). We further quantify the tight link between changes in ventilation and the non-thermal oxygen trends controlling oxygenation/deoxygenation patterns by computing the Pearson Correlation Coefficients between interannual anomalies in ideal age and non-thermal oxygen. Deviations from a correlation coefficient of unity can arise either

295  from changing biological oxygen demand or from the mixing of many source water masses (see Appendix B for details), while a coefficient of unity represents the special case where non-thermal oxygen trends are controlled by ventilation changes along a single pathway. Ventilation and non-thermal oxygen changes are well correlated (0.8-1.0) along the northern edge of the South Indian Gyre associated with Southern Pathway Waters (Feature 1), in the region of oxygenation in the South Equatorial Current (Feature 2) and in the northern Arabian Sea (Feature 3). Thus, there is strong evidence that changes in

300  physical ventilation pathways are the main control of features of dissolved oxygen change, and ultimately the reshaping of OMZ volume, in the Indian Ocean.

### 3.5 Shifts in water mass mixing control oxygenation in South Equatorial Current

In this and the following section, we attribute the significant features of projected oxygen trends in the Indian Ocean thermocline to specific changes in ventilation pathways. Perhaps the most remarkable aspect of projected dissolved oxygen changes in

305  the Indian Ocean under SSP5-8.5 forcing is the oxygenation dipole along the SEC. The two major ventilation pathways in this
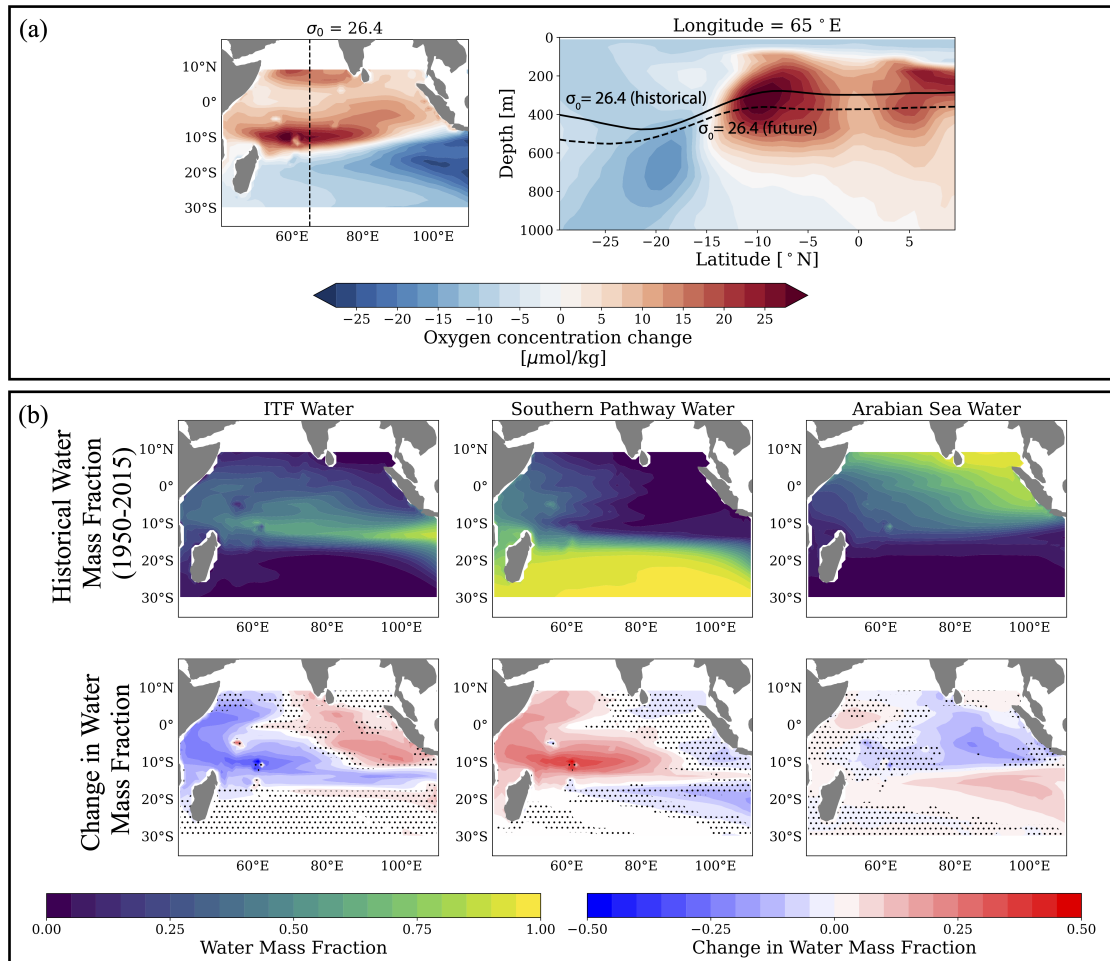
**Figure 8.** Multi-model mean (MMM) results of Optimum Multiparameter (OMP) mixing model in the South Equatorial Current. **(a)** Oxygen changes along the $\sigma_0 = 26.4$ surface and the historical (solid) and end-of-century (dashed) depth of $\sigma_0 = 26.4$ indicated over MMM oxygen changes in depth space at $65\,^\circ$E. **(b)** Historical distribution of Indonesian Throughflow, Southern Pathway, and Arabian Sea Water fractions, and changes in water mass fractions between historical and end-of-century states. Historical states calculated as 1950-2015 mean, and end-of-century states calculated as historical mean plus linear trends over 2015-2100. Stippling where less than 75% (6/8) of models agree on sign of change

region are the Southern Pathway Waters and Indonesian Throughflow Water. The transport of these two pathways is projected to decline between 100 and 1000 m over the twenty-first century (Fig. 7a). The transport of Southern Pathway Waters is projected to decline by $4.4\pm3.2\,\mathrm{Sv/century}$ and the transport of Indonesian Throughflow Waters by $5.1\pm2.0\,\mathrm{Sv/century}$ (Fig. 7a). The weakening of these transport pathways can easily explain the deoxygenation in the southeastern Indian Ocean where each pathway acts as a single dominant source (thus accounting for Feature 1). Curiously, however, this weakened transport seems

310

**15**

in apparent contradiction with the increased ventilation and oxygenation of the western South Equatorial Current (Fig. 4). We hypothesize that this oxygenation must arise from a shift in the mixing ratio between these source waters in the western South Equatorial Current where they co-dominate, favoring relatively young and oxygen-rich waters from the Southern Pathway over relatively old and oxygen-poor waters from the Indonesian Throughflow. To motivate this hypothesis, we show a time series of the ratio of inflowing volume transport from Southern Pathway Waters and Indonesian Throughflow Water at between 100 and 1000 m (Fig. 7b), demonstrating that this ratio increasingly favors Southern Pathway Waters over the twenty-first century. To test this hypothesis, we solve a mixing model (Tomczak and Large, 1989) in the tropical Indian Ocean for both a historical mean state (1950-2015) and an end-of-twenty-first-century mean state (climatological 2100) at a potential density layer within the thermocline, nominally $\sigma_0 = 26.4$ (Sect. 2.2.4). This potential density layer intersects the dipole of oxygen change (Features 1 and 2) in the South Equatorial Current (Fig. 8a). We solve for the mixing of three source waters: Indonesian Throughflow Water, Southern Pathway Waters and Arabian Sea Water (oxygen minimum water) (Sect. 2.2.4). The mixing model identifies a reasonable historical water mass distribution with Indonesian Throughflow Waters originating from the main straits of the Indonesian Throughflow and penetrating across the basin along $10°$ S, and Southern Pathway Waters residing primarily within the southern gyre until they join the western boundary current (Fig. 8b; in agreement with observed distribution from Tomczak and Large, 1989). Under SSP5-8.5 forcing, there is a significant shift in mixing ratios in the western South Equatorial Current away from Indonesian Throughflow Waters in favor of Southern Pathway Waters between the historical and future states. For instance, at $65°$ E and $10°$ S, Indonesian Throughflow Waters historically accounts for over 50% of the local water mass while Southern Pathway Waters accounts for about 10%. This shifts to nearly 50% Southern Pathway Waters and less than 30% Indonesian Throughflow Waters in the future state. Using nominal historical oxygen concentrations of each source water— 230, 135, and $40 \, \mu\mathrm{mol/kg}$ for Southern Pathway, Indonesian Throughflow , and Arabian Sea Waters, respectively— this shift in composition can account for about a $50 \, \mu\mathrm{mol/kg}$ increase in oxygen. This new water mass composition is then propagated across the equator by the western boundary current along the Somali coast and then East into the basin interior by the North Equatorial Current, increasing ventilation in the northern basin and accounting for the secondary oxygenation maximum north of the equator (Fig. 8). A previous study found that ESMs projected a strengthening of the cross-equatorial transport and North Equatorial Current with warming (Sharma et al., 2023), which may in turn strengthen the northern oxygenation maximum. We note that despite the movement of the $\sigma_0 = 26.4$ surface between the historical and end-of-century states, the results here are not an artifact of this isopycnal displacement (Fig S8)

### 3.6 Shoaling marginal sea outflows shift ventilation in the Arabian Sea

We perform a similar analysis as above to attribute the deoxygenation projected in the northern Arabian Sea (Feature 3) to changes in ventilation pathways, namely from marginal sea outflows. Unlike pathways in the southern Indian Ocean, the overall strength of marginal sea outflow transports remains steady under SSP5-8.5 forcing (Fig. 9). Neither the Persian Gulf outflow nor the Red Sea outflow show any robust trends in volume transport across the ESM ensemble. We hypothesize that, although overall transport from marginal seas does not change, the buoyancy of outflow plumes increases with the rapid heating of marginal seas, which can shoal the outflow plumes and reduce ventilation of the OMZ at thermocline depths. This hypothesis
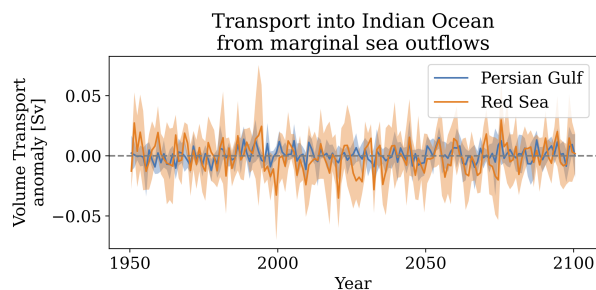
**Figure 9.** Interannual transport anomalies (referenced to 1950-2015 mean) of marginal sea outflows from Persian Gulf (blue) and Red Sea (orange). Solid curves represent multi-model mean (MMM) and shading represents one standard deviation of model spread. Transport data is available for 5 ESMs.

345    is motivated by the findings of Lachkar et al. (2019), who find that this mechanism can have a strong influence on the OMZ in the Arabian Sea. To test this, we solve a mixing model along the nominal potential density layer $\sigma_0 = 25.7$, which corresponds to the region of deoxygenation in the Arabian Sea (Feature 3; Fig. 10a). We define three source waters for the region: Persian Gulf Water, Red Sea Outflow Water and Arabian Sea Water (Sect. 2.2.4). In the historical state (1950-2015), Persian Gulf Water spreads from the Gulf of Oman across the northern Arabian Sea and Red Sea Water spreads from the Gulf of Aden,

350    while Arabian Sea Water acts as the ambient water in the basin (Fig. 10b). Concurrent with the region of deoxygenation in the northern Arabian Sea, there is a pronounced decrease in the presence of Persian Gulf Water in the end-of-century mean, which gets replaced by ambient Arabian Sea Water. In the historical state, Persian Gulf Water accounts for about 60% of the water mass at $65°\,$E, $23°\,$N, but this contribution is reduced to approximately 30% in the end-of-century state. This decrease in ventilation from the Persian Gulf Water can explain the deoxygenation simulated between 100 and 300 m. The mixing

355    model also suggests a decrease in ventilation from Red Sea Outflow Water along $\sigma_0 = 25.7$, which may contribute weakly to deoxygenation off of the Omani coast (Fig. 10b). We note that for an alternative analysis where the future state is evaluated at a potential density layer which aligns approximately with the historical depth of $\sigma_0 = 25.7$ (i.e., any aliasing from isopycnal displacement is removed; Sect. 2.2.4; Fig. S9), we see even greater agreement between the pattern of deoxygenation and decreases in Persian Gulf Water fraction.

360    ## 4  Discussion and Conclusions

We examine the changes in dissolved oxygen and OMZ volume in response to the high-emissions forcing (SSP5-8.5 scenario) in the Indian Ocean using an ensemble of eight CMIP6-generation Earth system models. In the following, we discuss the three regimes that characterize the OMZ response to warming in the Indian Ocean thermocline (upper 1000 m). We compare this response to that previously investigated for the Pacific Ocean OMZ and to the unstudied response for the Atlantic OMZ, and

365    contrast the OMZ changes projected in the thermocline to the changes projected in the deep ocean (Fig.11). We also revise
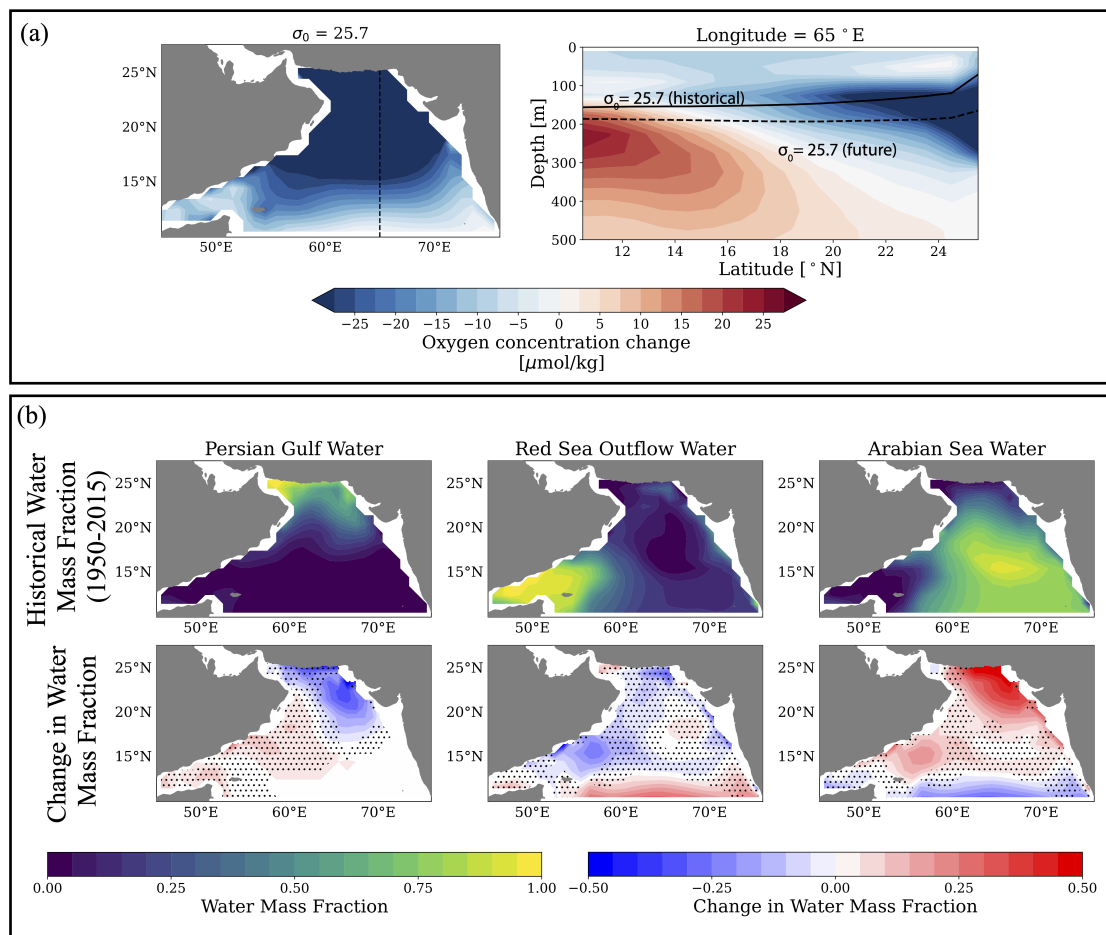
**Figure 10.** Multi-model mean (MMM) results of Optimum Multiparameter (OMP) mixing model in the Arabian Sea. **(a)** Oxygen changes along the $\sigma_0 = 25.7$ surface and the historical (solid) and end-of-century (dashed) depth of $\sigma_0 = 25.7$ indicated over MMM oxygen changes in depth space at $65\,^{\circ}$E. **(b)** Historical distribution of Persian Gulf, Red Sea Outflow, and Arabian Sea Water fractions, and changes in water mass fractions between historical and end-of-century states. Historical states calculated as 1950-2015 mean, and end-of-century states calculated as historical mean plus linear trends over 2015-2100. Stippling where less than 75% (6/8) of models agree on sign of change

the existing "single-pipe" and "mixing-network" ventilation framework to interpret the OMZ response of the Indian Ocean, discuss observational constraints on ventilation pathways, and consider caveats in the model ensemble projections.

## 4.1 Three-regime response of the oxygen minimum zone

The response of the OMZ in the Indian Ocean thermocline (upper 1000 m) falls into three regimes (Fig. 3a and 11a): a contraction of the OMZ delimited by low oxygen thresholds ($<85\,\mu\mathrm{mol/kg}$), an expansion of the OMZ delimited by high oxygen

thresholds ($>180\,\mu\mathrm{mol/kg}$), and a redistribution of the OMZ volume with relatively weak volume changes at intermediate oxygen thresholds (85 to $180\,\mu\mathrm{mol/kg}$). This three-regime response is similar to the OMZ response described in the Pacific Ocean by Busecke et al. (2022) (Fig. 11b). A striking difference between the two basins, however, is the widespread oxygen gain projected in the Indian Ocean. Indeed, ESMs robustly project an oxygenation of the OMZ cores in the Arabian Sea and
375 Bay of Bengal, similar to the Pacific OMZ core, but also an oxygenation of the southwest Indian Ocean along the path of the South Equatorial Current and North Equatorial Current. As a result, the OMZ contracts for thresholds as high as $85\,\mu\mathrm{mol/kg}$ (including the volume of hypoxic waters commonly defined by $60\,\mu\mathrm{mol/kg}$) in the Indian Ocean, whereas the contraction is restricted to the very low oxygen levels found in the OMZ core in the Pacific Ocean (typically volume with oxygen less than 10 to $20\,\mu\mathrm{mol/kg}$; Fig. 11a-b). The oxygen gain in the southwest Indian Ocean is associated with an oxygen loss in the southeast.
380 This dipole of southwest oxygenation and southeast deoxygenation along the path of the South Equatorial Current explains the redistribution regime and near zero volume change of the OMZ delimited by intermediate oxygen levels (85 to $180\,\mu\mathrm{mol/kg}$; Fig. 11b). Finally, upstream of the South Equatorial Current, the drastic decline in oxygen in the water masses that enter the thermocline through the South Indian Gyre and Indonesian Throughflow explains the expansion of OMZ volumes defined by high oxygen levels ($>180\,\mu\mathrm{mol/kg}$; Fig. 11a).

385 **4.2 Beyond "single-pipe" and "mixing-network": cases for "two-pipe" and "moving pipe" systems**

The projected oxygenation outside of the Indian OMZ core, or shadow zone, calls for a revision of the "single-pipe" and "mixing-network" ventilation framework used in the Pacific Ocean (Gnanadesikan et al., 2007). In the original framework, increased ventilation and oxygenation with weakened circulation was only reconcilable in shadow zones where there are no direct advective ventilation pathways and a mixing-network of multiple sources controls ventilation. In both the Pacific and
390 the Indian Oceans, the oxygenation of the OMZ core (which is associated with increased ventilation and reduced ideal age) can indeed be interpreted as a shift towards a stronger contribution from younger, oxygen-rich upper ocean waters using the mixing-network model (Bryan et al., 2006; Gnanadesikan et al., 2007, 2012; Takano et al., 2018; Busecke et al., 2022). In the Pacific, this effect has been attributed to a slowdown of Deep Waters upwelling to thermocline depths, and there is evidence of this same effect in the Indian Ocean basin. In the ESM ensemble used in this study, upwelling of Deep Waters across 1000
395 m weakens at a rate of $2.0\pm0.7\,\mathrm{Sv/century}$ in the Indian Ocean, even reversing sign to be net downwelling (under SSP5-8.5 forcing in this ESM ensemble, see Fig. S10).

Changes in mixing in the OMZ core are, however, not the primary effect driving oxygenation in the Indian Ocean. In the Southern Indian Ocean, ESMs project an oxygenation and increased ventilation well outside of the shadow zone, within regions of strong advection such as the South Equatorial Current. We show that this oxygenation can be interpreted as a "two-
400 pipe" system, an intermediate case between a "single-pipe" and a "mixing-network". Two sources with different oxygen levels, rather than a network of many sources, are in fact sufficient to have increased oxygenation, even though the transport by both ventilation sources weaken. The unique configuration of the Indonesian Throughflow and Southern Pathway merging into the South Equatorial Current allows for this phenomenon despite intense advection. The ventilation by the Southern Pathway and
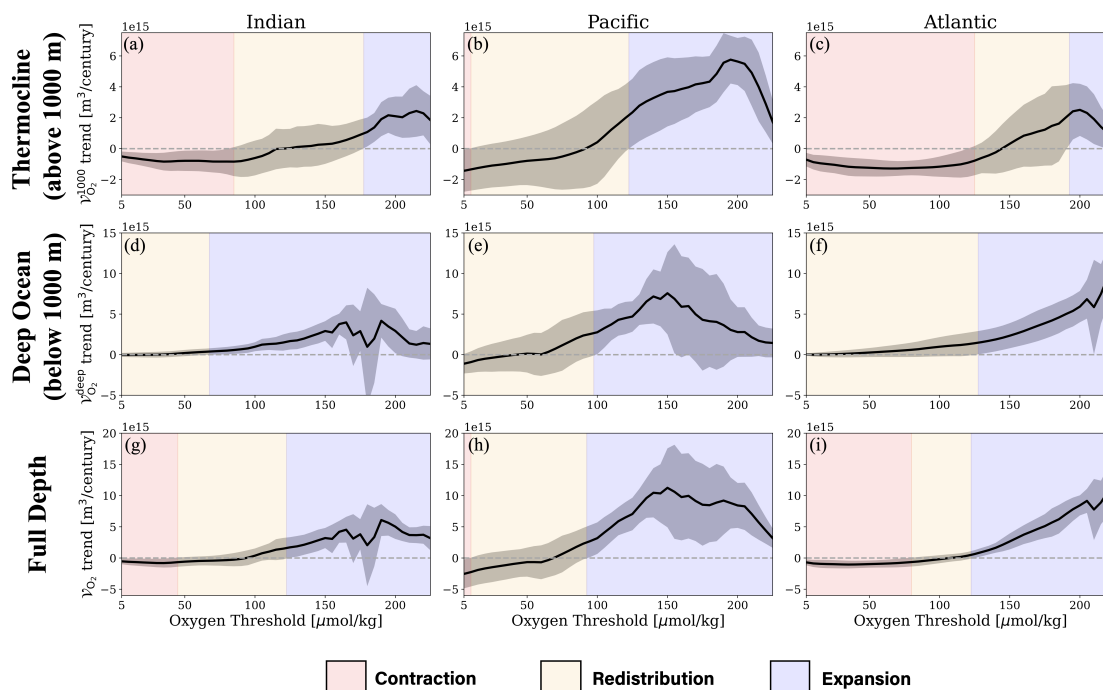
**Figure 11.** Multi-model mean thermocline OMZ volume trends (above 1000 m) under SSP5-8.5 scenario forcing (2015-2100) as a function of oxygen threshold for the tropical ($30°$ S - $30°$ N) **(a)** Indian, **(b)** Pacific and **(c)** Atlantic Oceans. Deep ocean (below 1000 m) OMZ volume trends for the tropical **(d)** Indian, **(e)** Pacific and **(c)** Atlantic Oceans. Full depth OMZ volume trends for the tropical **(g)** Indian, **(h)** Pacific and **(i)** Atlantic Oceans. Shading represents one standard deviation of model spread. Panel a is the same as Figure 3a

Indonesian Throughflow both decline in response to warming in the ESM ensemble, but the ventilation by the Indonesian
405　Throughflow declines more strongly, favoring the relative contribution of the better oxygenated Southern Pathway waters.

Another feature of the Indian Ocean OMZ response which differs from its Pacific Ocean counterpart is the importance of ventilation by marginal sea outflows. We find that changes in ventilation from marginal sea outflows are the main control of deoxygenation in the Arabian Sea. The Persian Gulf rapidly warms in response to global warming, increasing stratification and the buoyancy of outflow water from the Persian Gulf. As outflow water shoals, it becomes unable to ventilate the OMZ in
410　the Arabian Sea, and is instead confined to the upper 100 m where its impact on oxygen becomes marginal (the upper ocean is already well oxygenated; Lachkar et al., 2021). The deeper Red Sea outflow plume also shows evidence of shoaling in the ESM ensemble, but it has a weaker impact on the ventilation of the OMZ because its oxygen content is lower than that of the Persian Gulf (on average about $70\,\mu$mol/kg for Red Sea Outflow Water versus about $200\,\mu$mol/kg for Persian Gulf Water). We can describe this change in the ventilation from marginal seas as a "moving pipe", where oxygen supply may be affected
415　by a displacement of a pathway even if the strength of transport along a that pathway holds steady.

### 4.3 Global trends in tropical oxygen minimum zones

Now extending our scope to all tropical oceans, we find that the three-regime OMZ response identified in the Indian (this study) and Pacific (Busecke et al., 2022) Oceans is also simulated in the Atlantic Ocean (Fig. 11c). The dynamics driving this three-regime response in the Atlantic have not yet been explored in detail, but it is likely that the even more prominent

420    contraction regime found for the Atlantic OMZ is connected to ventilation by the Atlantic Meridional Overturning circulation, which is projected to weaken in ESMs (IPCC et al., 2013; Bakker et al., 2016). Looking beyond OMZ volume changes in the ocean thermocline (above 1000 m) to the deep ocean response (below 1000 m), we see that deoxygenation and OMZ expansion in the deep ocean are more ubiquitous than in the thermocline (Fig. 11d-f). Deoxygenation in the deep ocean is likely due to a slowdown of Deep Water transports as the global thermohaline circulation weakens with warming (e.g. Bakker

425    et al., 2016). When integrating the thermocline and deep ocean components of the OMZ response to consider the full depth of the water column (similar to what was done for the Pacific Ocean in Busecke et al., 2022), we find that the thermocline response dominates the OMZ contraction at low oxygen thresholds while the deep ocean response dominates the expansion at high thresholds (Fig. 11g-i).

### 4.4 Observational constraints and caveats

430    Projected oxygen changes, and thus OMZ volume changes are subject to uncertainties, in particular the magnitude of the oxygenation/deoxygenation dipole along the South Equatorial Current and the deoxygenation in the northern Arabian Sea. The slowdown of the Southern Pathway and Indonesian Throughflow transports is a robust and well studied feature of ESM projections (Downes et al., 2009; Sen Gupta et al., 2016; Feng et al., 2017; Stellema et al., 2019). Historical observations support the slowdown and deoxygenation of the Southern Pathway (Helm et al., 2011; Kobayashi et al., 2012; Ito et al., 2017;

435    McMonigal et al., 2022). A secular weakening of the Indonesian Throughflow has not yet been observed, possibly obscured by significant decadal variability (Liu et al., 2015; Feng et al., 2018), but there is evidence for forced trends in the global thermohaline circulation that controls the Indonesian Throughflow transport (Rahmstorf et al., 2015) to support the decline in ventilation by this pathway. However, the relative changes in the two pathways, which controls the oxygenation/deoxygenation dipole, is highly uncertain and unconstrained by observations. This dipole pattern has not emerged in current observation-based

440    estimates of historical oxygen trends (Helm et al., 2011; Ito et al., 2017; Schmidtko et al., 2017), though there is some signal of oxygenation near Madagascar in the product of Ito et al. (2017).

The rapid heating of marginal seas compared to the open ocean and the subsequent increase in stratification and buoyancy of the marginal sea outflows, particularly for the Persian Gulf is also supported by observations (Al-Yamani et al., 2017; Naqvi, 2021). The projected changes in outflow ventilation are consistent with the findings of ocean model simulation studies, which

445    showed that the warming and shoaling of the Persian Gulf was a major driver of the deoxygenation in the northern Arabian Sea (Lachkar et al., 2019, 2021). Yet, ESMs tend to overestimate the oxygen transport by these marginal sea outflows to the Arabian Sea (e.g. Schmidt et al., 2021, for CMIP5). This partially explains the systematic high oxygen bias in the Arabian Sea in the ensemble of eight CMIP6 ESMs used in this study (Fig. 1), the absence of an OMZ core in the five ESMs that were

excluded from the ensemble (Fig. S1,S2), and could influence the magnitude of the projected deoxygenation associated with

450 the vertical displacement of these outflows.

## 5  Conclusion

Oxygen minimum zones can be viewed as multiple concentric layers, like onions, with oxygen concentrations decreasing towards their core. Their response to deoxygenation and global warming in Earth system models falls into three regimes which are controlled by the mechanisms that ventilate these different layers: the outer layers of the oxygen minimum zone expand,

455 the inner layers contract, and in-between, oxygen is redistributed leading to near zero changes in volume but reshaping the spatial distribution of the intermediate layers. We show that this contrast between inner layer oxygenation and outer layer deoxygenation, which was first identified in the Pacific Ocean (e.g., Gnanadesikan et al., 2007; Busecke et al., 2022), applies to all tropical oxygen minimum zones. However, the unique geometry and ventilation pathways of the tropical Indian Ocean (bounded by continent to the north, Indonesian Throughflows and marginal seas) determine what layers of the oxygen minimum

460 zone experience contraction, redistribution and expansion. The Indian Ocean is characterized by a prominent oxygenation, attributed to changes in the ventilation by the Indonesian Throughflow, and consequently contraction and redistribution regimes that extend to a much larger range of oxygen minimum zone layers than its Pacific counterpart. Furthermore, the rapid warming and shoaling of marginal sea outflows leads to localized deoxygenation in the inner layers of the oxygen minimum zone of the northern Arabian Sea. We identify that the response of the Atlantic oxygen minimum zone also exhibits regimes of contraction,

465 redistribution, and expansion, but further investigations are required to understand the regional dynamics which produce a pronounced contraction response in that basin.

*Code and data availability.* The processed data files and code to reproduce results presented here are available at https://doi.org/10.5281/zenodo.7958387

## Appendix A: Extended Optimum Multiparameter Analysis

Extended Optimum Multiparameter Analysis (OMP; Karstensen and Tomczak, 1998) is a method of solving an over-determined

470 linear mixing model which takes into account the conversion of one tracer to another, generally by remineralization. Detailed explanations of the OMP method can be found in Tomczak and Large (1989) and Shrikumar et al. (2022), but here we give a brief summary.

First, we define a set of $N$ source water masses with properties, $p$. Let $e_p^i$ be the values for property $p$ and $i$-th source water mass. Each sample in the evaluation region has a value for each property, $s_p^j$. The goal is to solve for the fraction of $i$-th source

475 water masses in each sample, $x_i^j$. We can define the objective function:

$$\sum_{i=1}^{N} e_p^i x_i^j = s_p^j + \epsilon_p^j \tag{A1}$$

where $\epsilon_p^j$ is a residual to minimize. Using user defined weights, $W$, to assign relative importance to each property, the residual takes the form

$$\epsilon_p^j = \frac{W_p}{\sigma_p}\Big(\sum_i (e_p^i - \mu_p)x_i^j + r_B^A \Delta_j^B - (s_p^j - \mu_p)\Big) \tag{A2}$$

480  where we normalize and center the values for each property, $e_p^i$ with their mean, $\mu_p$, and variance, $\sigma_p$. We chose to set potential temperature and salinity fields weighted five times higher than dissolved oxygen fields in the mixing model's objective function because temperature and salinity tend to be the defining characteristics for source water masses. The results of the analysis are not sensitive to small changes in weight values. The term $r_B^A \Delta_j^B$ allows for the conservation of two properties, $A$ and $B$, which are exchanged via remineralization. Typically, this term is used to track conversion of oxygen to phosphorous, where $r$ is set to

485  be the Redfield Ratio. In this study, we simply allow for the conversion of oxygen to AOU with a ratio of $-1$. The cost function is thus defined as the sum of residuals for every property, $p$, as well as a mass conservation term $\epsilon_M^j$ which penalizes deviations from total mass fractions of unity for each sample point:

$$C^j = (\epsilon_M^j)^2 + \sum_p (\epsilon_p^j)^2 \tag{A3}$$

We note that the PyOMPA implementation of this method allows for a hard constraint on mass conservation, rather than

490  minimizing a residual (Shrikumar et al., 2022). However, we do not use this feature, and thus recover the original method of Karstensen and Tomczak (1998).

## Appendix B: Interpreting Pearson Correlations between AOU and Ideal Age anomalies

The Pearson Correlation Coefficient is a measure of linear correlation between two variables. Thus, for fields $x$ and $y$ related by the form $y = mx + \mathcal{N}$ for some constant $m$ and noise $\mathcal{N}$, the correlation coefficient is 1 if $\mathcal{N} = 0$.

495  Here, we derive the form of the noise term $\mathcal{N}$ for the linear relation between AOU and ideal age for a parcel of water. We assume the parcel of water can be made up of contributions from $N$ ventilation pathways, each with an average respiration rate $R$, ideal age $\tau$, and fractional contribution to the mass of the parcel $f$. AOU and ideal age of the parcel is thus modeled as:

$$\overline{AOU} = \overline{R\tau} = \sum_i^N f_i R_i \tau_i \tag{B1}$$

$$\overline{\tau} = \sum_i^N f_i \tau_i \tag{B2}$$

500  Changes in AOU and ideal age are modeled as

$$\Delta\overline{AOU} = \sum_i^N (\Delta f_i R_i \tau_i + f_i \Delta R_i \tau_i + f_i R_i \Delta \tau_i) \tag{B3}$$

$$\Delta\overline{\tau} = \sum_i^N (\Delta f_i \tau_i + f_i \Delta \tau_i) \tag{B4}$$

Rearranging,

$$\Delta\overline{AOU} = \sum_i^N (\Delta f_i R_i \tau_i + f_i R_i \Delta \tau_i + f_i \Delta R_i \tau_i) \tag{B5}$$

$$= \sum_i^N R_i \sum_i^N (\Delta f_i \tau_i + f_i \Delta \tau_i) - \sum_{i \neq j}^N f_j R_i \Delta \tau_j - \sum_{i \neq j}^N \Delta f_j R_i \tau_j + \sum_i^N f_i \Delta R_i \tau_i \tag{B6}$$

$$= \Delta\overline{\tau} \sum_i^N R_i - \sum_{i \neq j}^N f_j R_i \Delta \tau_j - \sum_{i \neq j}^N \Delta f_j R_i \tau_j + \sum_i^N f_i \Delta R_i \tau_i \tag{B7}$$

Thus, we can relate AOU and ideal age changes of the parcel in the form $\Delta\overline{AOU} = m\Delta\overline{\tau} + \mathcal{N}$, where

$$m = \sum_i^N R_i \tag{B8}$$

and

$$\mathcal{N} = \sum_i^N f_i \Delta R_i \tau_i - \sum_{i \neq j}^N (f_j R_i \Delta \tau_j + \Delta f_j R_i \tau_j) \tag{B9}$$

The two terms in $\mathcal{N}$ respectively represent changes in respiration rates along each pathway and a loss of information on constituent pathways in the averaged signal. So, a correlation coefficient of 1 between AOU and ideal age changes represent the special case where changes occur along a single pathway and respiration rates remain constant.

*Competing interests.* The authors declare no conflicts of interest relevant to this study.

# References

Al-Yamani, F., Yamamoto, T., Al-Said, T., and Alghunaim, A.: Dynamic hydrographic variations in northwestern Arabian Gulf over the past three decades: Temporal shifts and trends derived from long-term monitoring data, Marine Pollution Bulletin, 122, 488–499, 2017.

Auderset, A., Moretti, S., Taphorn, B., Ebner, P.-R., Kast, E., Wang, X. T., Schiebel, R., Sigman, D. M., Haug, G. H., and Martínez-García, A.: Enhanced ocean oxygenation during Cenozoic warm periods, Nature, 609, 77–82, 2022.

Bakker, P., Schmittner, A., Lenaerts, J., Abe-Ouchi, A., Bi, D., van den Broeke, M., Chan, W.-L., Hu, A., Beadling, R., Marsland, S., et al.: Fate of the Atlantic Meridional Overturning Circulation: Strong decline under continued warming and Greenland melting, Geophysical Research Letters, 43, 12–252, 2016.

Banse, K., Naqvi, S., Narvekar, P., Postel, J., and Jayakumar, D.: Oxygen minimum zone of the open Arabian Sea: variability of oxygen and nitrite from daily to decadal timescales, Biogeosciences, 11, 2237–2261, 2014.

Beal, L. M., Ffield, A., and Gordon, A. L.: Spreading of Red Sea overflow waters in the Indian Ocean, Journal of Geophysical Research: Oceans, 105, 8549–8564, 2000.

Bentsen, M., Oliviè, D. J. L., Seland, y., Toniazzo, T., Gjermundsen, A., Graff, L. S., Debernard, J. B., Gupta, A. K., He, Y., Kirkevåg, A., Schwinger, J., Tjiputra, J., Aas, K. S., Bethke, I., Fan, Y., Griesfeller, J., Grini, A., Guo, C., Ilicak, M., Karset, I. H. H., Landgren, O. A., Liakka, J., Moseid, K. O., Nummelin, A., Spensberger, C., Tang, H., Zhang, Z., Heinze, C., Iversen, T., and Schulz, M.: NCC NorESM2-MM model output prepared for CMIP6 CMIP, https://doi.org/10.22033/ESGF/CMIP6.506, 2019a.

Bentsen, M., Oliviè, D. J. L., Seland, y., Toniazzo, T., Gjermundsen, A., Graff, L. S., Debernard, J. B., Gupta, A. K., He, Y., Kirkevåg, A., Schwinger, J., Tjiputra, J., Aas, K. S., Bethke, I., Fan, Y., Griesfeller, J., Grini, A., Guo, C., Ilicak, M., Karset, I. H. H., Landgren, O. A., Liakka, J., Moseid, K. O., Nummelin, A., Spensberger, C., Tang, H., Zhang, Z., Heinze, C., Iversen, T., and Schulz, M.: NCC NorESM2-MM model output prepared for CMIP6 ScenarioMIP, https://doi.org/10.22033/ESGF/CMIP6.608, 2019b.

Bertrand, A., Chaigneau, A., Peraltilla, S., Ledesma, J., Graco, M., Monetti, F., and Chavez, F. P.: Oxygen: a fundamental property regulating pelagic ecosystem structure in the coastal southeastern tropical Pacific, PloS one, 6, e29 558, 2011.

Bindoff, N. L., Cheung, W. W., Kairo, J. G., Arístegui, J., Guinder, V. A., Hallberg, R., Hilmi, N. J. M., Jiao, N., Karim, M. S., Levin, L., et al.: Changing ocean, marine ecosystems, and dependent communities, IPCC special report on the ocean and cryosphere in a changing climate, pp. 477–587, 2019.

Bopp, L., Resplandy, L., Orr, J. C., Doney, S. C., Dunne, J. P., Gehlen, M., Halloran, P., Heinze, C., Ilyina, T., Seferian, R., et al.: Multiple stressors of ocean ecosystems in the 21st century: projections with CMIP5 models, Biogeosciences, 10, 6225–6245, 2013.

Bopp, L., Resplandy, L., Untersee, A., Le Mezo, P., and Kageyama, M.: Ocean (de) oxygenation from the Last Glacial Maximum to the twenty-first century: insights from Earth System models, Philosophical Transactions of the Royal Society A: Mathematical, Physical and Engineering Sciences, 375, 20160 323, 2017.

Bouchard, C. and Crumplin, W.: Neglected no longer: the Indian Ocean at the forefront of world geopolitics and global geostrategy, Journal of the Indian Ocean Region, 6, 26–51, 2010.

Brandt, P., Bange, H. W., Banyte, D., Dengler, M., Didwischus, S.-H., Fischer, T., Greatbatch, R. J., Hahn, J., Kanzow, T., Karstensen, J., et al.: On the role of circulation and mixing in the ventilation of oxygen minimum zones with a focus on the eastern tropical North Atlantic, Biogeosciences, 12, 489–512, 2015.

Brill, R. W.: Selective advantages conferred by the high performance physiology of tunas, billfishes, and dolphin fish, Comparative Biochemistry and Physiology Part A: Physiology, 113, 3–15, 1996.

Bryan, F. O., Danabasoglu, G., Gent, P. R., and Lindsay, K.: Changes in ocean ventilation during the 21st century in the CCSM3, Ocean Modelling, 15, 141–156, 2006.

565 Busecke, J. J., Resplandy, L., Ditkovsky, S. J., and John, J. G.: Diverging fates of the Pacific Ocean oxygen minimum zone and its core in a warming world, AGU Advances, 3, e2021AV000 470, 2022.

Busecke, J. J. M. and Spring, A.: jbusecke/cmip6_preprocessing: v0.1.4, https://doi.org/10.5281/zenodo.3743397, 2020.

Cabré, A., Marinov, I., Bernardello, R., and Bianchi, D.: Oxygen minimum zones in the tropical Pacific across CMIP5 models: mean state differences and climate change trends, Biogeosciences, 12, 5429–5454, 2015.

570 Clifton, J., Etienne, M., Barnes, D. K., Barnes, R. S., Suggett, D. J., and Smith, D. J.: Marine conservation policy in Seychelles: Current constraints and prospects for improvement, Marine Policy, 36, 823–831, 2012.

Cocco, V., Joos, F., Steinacher, M., Frölicher, T. L., Bopp, L., Dunne, J., Gehlen, M., Heinze, C., Orr, J., Oschlies, A., et al.: Oxygen and indicators of stress for marine life in multi-model global warming projections, Biogeosciences, 10, 1849–1868, 2013.

Deutsch, C., Berelson, W., Thunell, R., Weber, T., Tems, C., McManus, J., Crusius, J., Ito, T., Baumgartner, T., Ferreira, V., et al.: Centennial
575  changes in North Pacific anoxia linked to tropical trade winds, Science, 345, 665–668, 2014.

Deutsch, C., Penn, J. L., and Seibel, B.: Metabolic trait diversity shapes marine biogeography, Nature, 585, 557–562, 2020.

Downes, S. M., Bindoff, N. L., and Rintoul, S. R.: Impacts of climate change on the subduction of mode and intermediate water masses in the Southern Ocean, Journal of Climate, 22, 3289–3302, 2009.

Dueri, S., Bopp, L., and Maury, O.: Projecting the impacts of climate change on skipjack tuna abundance and spatial distribution, Global
580  Change Biology, 20, 742–753, 2014.

Duteil, O., Böning, C. W., and Oschlies, A.: Variability in subtropical-tropical cells drives oxygen levels in the tropical Pacific Ocean, Geophysical Research Letters, 41, 8926–8934, 2014.

Duteil, O., Frenger, I., and Getzlaff, J.: The riddle of eastern tropical Pacific Ocean oxygen levels: the role of the supply by intermediate-depth waters, Ocean Science, 17, 1489–1507, 2021.

585 Eyring, V., Bony, S., Meehl, G. A., Senior, C. A., Stevens, B., Stouffer, R. J., and Taylor, K. E.: Overview of the Coupled Model Intercomparison Project Phase 6 (CMIP6) experimental design and organization, Geoscientific Model Development, 9, 1937–1958, 2016.

Feng, M., Zhang, X., Sloyan, B., and Chamberlain, M.: Contribution of the deep ocean to the centennial changes of the Indonesian Throughflow, Geophysical Research Letters, 44, 2859–2867, 2017.

Feng, M., Zhang, N., Liu, Q., and Wijffels, S.: The Indonesian throughflow, its variability and centennial change, Geoscience Letters, 5,
590  1–10, 2018.

Fine, R. A.: Circulation of Antarctic intermediate water in the South Indian Ocean, Deep Sea Research Part I: Oceanographic Research Papers, 40, 2021–2042, 1993.

Firing, E., Fernandes, F., Barna, A., and Abernathey, R.: GSW-python: Python implementation of the Thermodynamic Equation of Seawater 2010 (TEOS-10), Zenodo [code], 2021.

595 Garcia, H., Weathers, K., Paver, C., Smolyar, I., Boyer, T., Locarnini, M., Zweng, M., Mishonov, A., Baranova, O., Seidov, D., et al.: World Ocean Atlas 2018, Volume 3: Dissolved Oxygen, Apparent Oxygen Utilization, and Dissolved Oxygen Saturation., 2019.

Gattuso, J.-P., Magnan, A., Billé, R., Cheung, W. W., Howes, E. L., Joos, F., Allemand, D., Bopp, L., Cooley, S. R., Eakin, C. M., et al.: Contrasting futures for ocean and society from different anthropogenic $CO_2$ emissions scenarios, Science, 349, aac4722, 2015.

Gnanadesikan, A., Russell, J., and Zeng, F.: How does ocean ventilation change under global warming?, Ocean Science, 3, 43–53, 2007.

600   Gnanadesikan, A., Dunne, J., and John, J.: Understanding why the volume of suboxic waters does not increase over centuries of global
      warming in an Earth System Model, Biogeosciences, 9, 1159–1172, 2012.

      Gnanadesikan, A., Bianchi, D., and Pradal, M.-A.: Critical role for mesoscale eddy diffusion in supplying oxygen to hypoxic ocean waters,
      Geophysical Research Letters, 40, 5194–5198, 2013.

      Good, P., Sellar, A., Tang, Y., Rumbold, S., Ellis, R., Kelley, D., Kuhlbrodt, T., and Walton, J.: MOHC UKESM1.0-LL model output prepared
605   for CMIP6 ScenarioMIP, https://doi.org/10.22033/ESGF/CMIP6.1567, 2019.

      Guo, H., John, J. G., Blanton, C., McHugh, C., Nikonov, S., Radhakrishnan, A., Rand, K., Zadeh, N. T., Balaji, V., Durachta, J., Dupuis, C.,
      Menzel, R., Robinson, T., Underwood, S., Vahlenkamp, H., Bushuk, M., Dunne, K. A., Dussin, R., Gauthier, P. P., Ginoux, P., Griffies,
      S. M., Hallberg, R., Harrison, M., Hurlin, W., Lin, P., Malyshev, S., Naik, V., Paulot, F., Paynter, D. J., Ploshay, J., Reichl, B. G.,
      Schwarzkopf, D. M., Seman, C. J., Shao, A., Silvers, L., Wyman, B., Yan, X., Zeng, Y., Adcroft, A., Dunne, J. P., Held, I. M., Krast-
610   ing, J. P., Horowitz, L. W., Milly, P., Shevliakova, E., Winton, M., Zhao, M., and Zhang, R.: NOAA-GFDL GFDL-CM4 model output,
      https://doi.org/10.22033/ESGF/CMIP6.1402, 2018a.

      Guo, H., John, J. G., Blanton, C., McHugh, C., Nikonov, S., Radhakrishnan, A., Rand, K., Zadeh, N. T., Balaji, V., Durachta, J., Dupuis,
      C., Menzel, R., Robinson, T., Underwood, S., Vahlenkamp, H., Dunne, K. A., Gauthier, P. P., Ginoux, P., Griffies, S. M., Hallberg,
      R., Harrison, M., Hurlin, W., Lin, P., Malyshev, S., Naik, V., Paulot, F., Paynter, D. J., Ploshay, J., Schwarzkopf, D. M., Seman, C. J.,
615   Shao, A., Silvers, L., Wyman, B., Yan, X., Zeng, Y., Adcroft, A., Dunne, J. P., Held, I. M., Krasting, J. P., Horowitz, L. W., Milly, C.,
      Shevliakova, E., Winton, M., Zhao, M., and Zhang, R.: NOAA-GFDL GFDL-CM4 model output prepared for CMIP6 ScenarioMIP,
      https://doi.org/10.22033/ESGF/CMIP6.9242, 2018b.

      Hajima, T., Abe, M., Arakawa, O., Suzuki, T., Komuro, Y., Ogura, T., Ogochi, K., Watanabe, M., Yamamoto, A., Tatebe, H., Noguchi, M. A.,
      Ohgaito, R., Ito, A., Yamazaki, D., Ito, A., Takata, K., Watanabe, S., Kawamiya, M., and Tachiiri, K.: MIROC MIROC-ES2L model output
620   prepared for CMIP6 CMIP, https://doi.org/10.22033/ESGF/CMIP6.902, 2019.

      Harper, S.: Thermocline ventilation and pathways of tropical–subtropical water mass exchange, Tellus A: Dynamic Meteorology and
      Oceanography, 52, 330–345, 2000.

      Helm, K. P., Bindoff, N. L., and Church, J. A.: Observed decreases in oxygen content of the global ocean, Geophysical Research Letters, 38,
      2011.

625   IPCC, A. et al.: Climate change 2013: the physical science basis, Contribution of working group I to the fifth assessment report of the
      intergovernmental panel on climate change, 1535, 2013.

      Ito, T., Minobe, S., Long, M. C., and Deutsch, C.: Upper ocean O2 trends: 1958–2015, Geophysical Research Letters, 44, 4214–4223, 2017.

      John, J. G., Blanton, C., McHugh, C., Radhakrishnan, A., Rand, K., Vahlenkamp, H., Wilson, C., Zadeh, N. T., Dunne, J. P., Dussin, R.,
      Horowitz, L. W., Krasting, J. P., Lin, P., Malyshev, S., Naik, V., Ploshay, J., Shevliakova, E., Silvers, L., Stock, C., Winton, M., and Zeng,
630   Y.: NOAA-GFDL GFDL-ESM4 model output prepared for CMIP6 ScenarioMIP, https://doi.org/10.22033/ESGF/CMIP6.1414, 2018.

      Jungclaus, J., Bittner, M., Wieners, K.-H., Wachsmann, F., Schupfner, M., Legutke, S., Giorgetta, M., Reick, C., Gayler, V., Haak, H.,
      de Vrese, P., Raddatz, T., Esch, M., Mauritsen, T., von Storch, J.-S., Behrens, J., Brovkin, V., Claussen, M., Crueger, T., Fast, I., Fiedler,
      S., Hagemann, S., Hohenegger, C., Jahns, T., Kloster, S., Kinne, S., Lasslop, G., Kornblueh, L., Marotzke, J., Matei, D., Meraner, K.,
      Mikolajewicz, U., Modali, K., Müller, W., Nabel, J., Notz, D., Peters, K., Pincus, R., Pohlmann, H., Pongratz, J., Rast, S., Schmidt, H.,
635   Schnur, R., Schulzweida, U., Six, K., Stevens, B., Voigt, A., and Roeckner, E.: MPI-M MPIESM1.2-HR model output prepared for CMIP6
      CMIP, https://doi.org/10.22033/ESGF/CMIP6.741, 2019.

Karstensen, J. and Quadfasel, D.: Water subducted into the Indian Ocean subtropical gyre, Deep Sea Research Part II: Topical Studies in Oceanography, 49, 1441–1457, 2002.

Karstensen, J. and Tomczak, M.: Ventilation processes and water mass ages in the thermocline of the southeast Indian Ocean, Geophysical
640     Research Letters, 24, 2777–2780, 1997.

Karstensen, J. and Tomczak, M.: Age determination of mixed water masses using CFC and oxygen data, Journal of Geophysical Research: Oceans, 103, 18 599–18 609, 1998.

Keeling, R. F., Körtzinger, A., Gruber, N., et al.: Ocean deoxygenation in a warming world, Annu. Rev. Mar. Sci, 2, 199–229, 2010.

Kobayashi, T., Mizuno, K., and Suga, T.: Long-term variations of surface and intermediate waters in the southern Indian Ocean along 32 S,
645     Journal of oceanography, 68, 243–265, 2012.

Krasting, J. P., John, J. G., Blanton, C., McHugh, C., Nikonov, S., Radhakrishnan, A., Rand, K., Zadeh, N. T., Balaji, V., Durachta, J., Dupuis, C., Menzel, R., Robinson, T., Underwood, S., Vahlenkamp, H., Dunne, K. A., Gauthier, P. P., Ginoux, P., Griffies, S. M., Hallberg, R., Harrison, M., Hurlin, W., Malyshev, S., Naik, V., Paulot, F., Paynter, D. J., Ploshay, J., Reichl, B. G., Schwarzkopf, D. M., Seman, C. J., Silvers, L., Wyman, B., Zeng, Y., Adcroft, A., Dunne, J. P., Dussin, R., Guo, H., He, J., Held, I. M., Horowitz, L. W., Lin, P., Milly, P.,
650     Shevliakova, E., Stock, C., Winton, M., Wittenberg, A. T., Xie, Y., and Zhao, M.: NOAA-GFDL GFDL-ESM4 model output prepared for CMIP6 CMIP, https://doi.org/10.22033/ESGF/CMIP6.1407, 2018.

Kwiatkowski, L., Torres, O., Bopp, L., Aumont, O., Chamberlain, M., Christian, J. R., Dunne, J. P., Gehlen, M., Ilyina, T., John, J. G., et al.: Twenty-first century ocean warming, acidification, deoxygenation, and upper-ocean nutrient and primary production decline from CMIP6 model projections, Biogeosciences, 17, 3439–3470, 2020.

655     Lachkar, Z., Smith, S., Lévy, M., and Pauluis, O.: Eddies reduce denitrification and compress habitats in the Arabian Sea, Geophysical Research Letters, 43, 9148–9156, 2016.

Lachkar, Z., Lévy, M., and Smith, K. S.: Strong intensification of the Arabian Sea oxygen minimum zone in response to Arabian Gulf warming, Geophysical Research Letters, 46, 5420–5429, 2019.

Lachkar, Z., Mehari, M., Al Azhar, M., Lévy, M., and Smith, S.: Fast local warming is the main driver of recent deoxygenation in the northern
660     Arabian Sea, Biogeosciences, 18, 5831–5849, 2021.

Levin, L. A.: Manifestation, drivers, and emergence of open ocean deoxygenation, Annual review of marine science, 10, 229–260, 2018.

Lévy, M., Resplandy, L., Palter, J. B., Couespel, D., and Lachkar, Z.: The crucial contribution of mixing to present and future ocean oxygen distribution, in: Ocean mixing, pp. 329–344, Elsevier, 2022.

Liu, Q.-Y., Feng, M., Wang, D., and Wijffels, S.: Interannual variability of the I ndonesian T hroughflow transport: A revisit based on 30 year
665     expendable bathythermograph data, Journal of Geophysical Research: Oceans, 120, 8270–8282, 2015.

Llanillo, P., Pelegrí, J. L., Talley, L., Peña-Izquierdo, J., and Cordero, R.: Oxygen pathways and budget for the eastern South Pacific oxygen minimum zone, Journal of Geophysical Research: Oceans, 123, 1722–1744, 2018.

Llewellyn, L. E., English, S., and Barnwell, S.: A roadmap to a sustainable Indian Ocean blue economy, Journal of the Indian Ocean Region, 12, 52–66, 2016.

670     Luyten, J., Pedlosky, J., and Stommel, H.: The ventilated thermocline, Journal of Physical Oceanography, 13, 292–309, 1983.

Margolskee, A., Frenzel, H., Emerson, S., and Deutsch, C.: Ventilation pathways for the North Pacific oxygen deficient zone, Global Biogeochemical Cycles, 33, 875–890, 2019.

McCarthy, M. C. and Talley, L. D.: Three-dimensional isoneutral potential vorticity structure in the Indian Ocean, Journal of Geophysical Research: Oceans, 104, 13 251–13 267, 1999.

675 McCarthy, M. C., Talley, L. D., and Baringer, M. O.: Deep upwelling and diffusivity in the southern Central Indian Basin, Geophysical Research Letters, 24, 2801–2804, 1997.

McMonigal, K., Gunn, K. L., Beal, L. M., Elipot, S., and Willis, J. K.: Reduction in meridional heat export contributes to recent Indian Ocean warming, Journal of physical oceanography, 52, 329–345, 2022.

Menezes, V. V.: Advective pathways and transit times of the Red Sea Overflow Water in the Arabian Sea from Lagrangian simulations,
680 Progress in Oceanography, 199, 102 697, 2021.

Miller, D., Poucher, S., and Coiro, L.: Determination of lethal dissolved oxygen levels for selected marine and estuarine fishes, crustaceans, and a bivalve, Marine Biology, 140, 287–296, 2002.

Naqvi, S. W. A.: Deoxygenation in marginal seas of the Indian ocean, Frontiers in Marine Science, 8, 624 322, 2021.

Nicholas, T., Busecke, J., and Abernathey, R.: xGCM: Staggered Grids, Topologies, and Ufuncs in Python, in: 103rd AMS Annual Meeting,
685 AMS, 2023.

O'Neill, B. C., Tebaldi, C., Van Vuuren, D. P., Eyring, V., Friedlingstein, P., Hurtt, G., Knutti, R., Kriegler, E., Lamarque, J.-F., Lowe, J., et al.: The scenario model intercomparison project (ScenarioMIP) for CMIP6, Geoscientific Model Development, 9, 3461–3482, 2016.

Oschlies, A., Schulz, K. G., Riebesell, U., and Schmittner, A.: Simulated 21st century's increase in oceanic suboxia by CO2-enhanced biotic carbon export, Global Biogeochemical Cycles, 22, 2008.

690 Oschlies, A., Brandt, P., Stramma, L., and Schmidtko, S.: Drivers and mechanisms of ocean deoxygenation, Nature Geoscience, 11, 467–473, 2018.

Paulmier, A. and Ruiz-Pino, D.: Oxygen minimum zones (OMZs) in the modern ocean, Progress in Oceanography, 80, 113–128, 2009.

Pedlosky, J.: Eastern boundary ventilation and the structure of the thermocline, Journal of physical oceanography, 13, 2038–2044, 1983.

Phillips, H. E., Tandon, A., Furue, R., Hood, R., Ummenhofer, C. C., Benthuysen, J. A., Menezes, V., Hu, S., Webber, B., Sanchez-Franks,
695 A., et al.: Progress in understanding of Indian Ocean circulation, variability, air–sea exchange, and impacts on biogeochemistry, Ocean Science, 17, 1677–1751, 2021.

Piontkovski, S. and Al-Oufi, H.: The Omani shelf hypoxia and the warming Arabian Sea, International Journal of Environmental Studies, 72, 256–264, 2015.

Prince, E. D. and Goodyear, C. P.: Hypoxia-based habitat compression of tropical pelagic fishes, Fisheries Oceanography, 15, 451–464, 2006.

700 Queste, B. Y., Vic, C., Heywood, K. J., and Piontkovski, S. A.: Physical controls on oxygen distribution and denitrification potential in the north west Arabian Sea, Geophysical Research Letters, 45, 4143–4152, 2018.

Rahmstorf, S., Box, J. E., Feulner, G., Mann, M. E., Robinson, A., Rutherford, S., and Schaffernicht, E. J.: Exceptional twentieth-century slowdown in Atlantic Ocean overturning circulation, Nature climate change, 5, 475–480, 2015.

Resplandy, L.: Will ocean zones with low oxygen levels expand or shrink?, 2018.

705 Resplandy, L., Lévy, M., Bopp, L., Echevin, V., Pous, S., Sarma, V., and Kumar, D.: Controlling factors of the oxygen balance in the Arabian Sea's OMZ, Biogeosciences, 9, 5095–5109, 2012.

Rhein, M., Stramma, L., and Plähn, O.: Tracer signals of the intermediate layer of the Arabian Sea, Geophysical research letters, 24, 2561–2564, 1997.

Rixen, T., Cowie, G., Gaye, B., Goes, J., do Rosário Gomes, H., Hood, R. R., Lachkar, Z., Schmidt, H., Segschneider, J., and Singh, A.:
710 Present past and future of the OMZ in the northern Indian Ocean, Biogeosci. Discuss, 10, 2020.

Roxy, M. K., Ritika, K., Terray, P., and Masson, S.: The curious case of Indian Ocean warming, Journal of Climate, 27, 8501–8509, 2014.

Roy, A.: Blue economy in the Indian Ocean: Governance perspectives for sustainable development in the region, ORF Occasional Paper, 181, 2019.

Schmidt, H., Getzlaff, J., Löptien, U., and Oschlies, A.: Causes of uncertainties in the representation of the Arabian Sea oxygen minimum
715     zone in CMIP5 models, Ocean Science, 17, 1303–1320, 2021.

Schmidtko, S., Stramma, L., and Visbeck, M.: Decline in global oceanic oxygen content during the past five decades, Nature, 542, 335–339, 2017.

Schott, F. A., Dengler, M., and Schoenefeldt, R.: The shallow overturning circulation of the Indian Ocean, Progress in oceanography, 53, 57–103, 2002.

720   Schott, F. A., Xie, S.-P., and McCreary Jr, J. P.: Indian Ocean circulation and climate variability, Reviews of Geophysics, 47, 2009.

Schupfner, M., Wieners, K.-H., Wachsmann, F., Steger, C., Bittner, M., Jungclaus, J., Früh, B., Pankatz, K., Giorgetta, M., Reick, C., Legutke, S., Esch, M., Gayler, V., Haak, H., de Vrese, P., Raddatz, T., Mauritsen, T., von Storch, J.-S., Behrens, J., Brovkin, V., Claussen, M., Crueger, T., Fast, I., Fiedler, S., Hagemann, S., Hohenegger, C., Jahns, T., Kloster, S., Kinne, S., Lasslop, G., Kornblueh, L., Marotzke, J., Matei, D., Meraner, K., Mikolajewicz, U., Modali, K., Müller, W., Nabel, J., Notz, D., Peters, K., Pincus, R., Pohlmann, H., Pongratz,
725     J., Rast, S., Schmidt, H., Schnur, R., Schulzweida, U., Six, K., Stevens, B., Voigt, A., and Roeckner, E.: DKRZ MPI-ESM1.2-HR model output prepared for CMIP6 ScenarioMIP, https://doi.org/10.22033/ESGF/CMIP6.2450, 2019.

Seland, y., Bentsen, M., Oliviè, D. J. L., Toniazzo, T., Gjermundsen, A., Graff, L. S., Debernard, J. B., Gupta, A. K., He, Y., Kirkevåg, A., Schwinger, J., Tjiputra, J., Aas, K. S., Bethke, I., Fan, Y., Griesfeller, J., Grini, A., Guo, C., Ilicak, M., Karset, I. H. H., Landgren, O. A., Liakka, J., Moseid, K. O., Nummelin, A., Spensberger, C., Tang, H., Zhang, Z., Heinze, C., Iversen, T., and Schulz, M.: NCC
730     NorESM2-LM model output prepared for CMIP6 CMIP, https://doi.org/10.22033/ESGF/CMIP6.502, 2019a.

Seland, y., Bentsen, M., Oliviè, D. J. L., Toniazzo, T., Gjermundsen, A., Graff, L. S., Debernard, J. B., Gupta, A. K., He, Y., Kirkevåg, A., Schwinger, J., Tjiputra, J., Aas, K. S., Bethke, I., Fan, Y., Griesfeller, J., Grini, A., Guo, C., Ilicak, M., Karset, I. H. H., Landgren, O. A., Liakka, J., Moseid, K. O., Nummelin, A., Spensberger, C., Tang, H., Zhang, Z., Heinze, C., Iversen, T., and Schulz, M.: NCC NorESM2-LM model output prepared for CMIP6 ScenarioMIP, https://doi.org/10.22033/ESGF/CMIP6.604, 2019b.

735   Sen Gupta, A., McGregor, S., Van Sebille, E., Ganachaud, A., Brown, J. N., and Santoso, A.: Future changes to the Indonesian Throughflow and Pacific circulation: The differing role of wind and deep circulation changes, Geophysical Research Letters, 43, 1669–1678, 2016.

Sharma, S., Ha, K.-J., Yamaguchi, R., Rodgers, K. B., Timmermann, A., and Chung, E.-S.: Future Indian Ocean warming patterns, Nature Communications, 14, 1789, 2023.

Sheehan, P. M., Webber, B. G., Sanchez-Franks, A., Matthews, A. J., Heywood, K. J., and Vinayachandran, P.: Injection of oxygenated
740     Persian Gulf Water into the southern Bay of Bengal, Geophysical Research Letters, 47, e2020GL087 773, 2020.

Shrikumar, A., Lawrence, R., and Casciotti, K. L.: PYOMPA version 0.3, Authorea Preprints, 2022.

Sofianos, S. S. and Johns, W. E.: Observations of the summer Red Sea circulation, Journal of Geophysical Research: Oceans, 112, 2007.

Sprintall, J. and Tomczak, M.: On the formation of Central Water and thermocline ventilation in the southern hemisphere, Deep Sea Research Part I: Oceanographic Research Papers, 40, 827–848, 1993.

745   Sprintall, J., Wijffels, S. E., Molcard, R., and Jaya, I.: Direct estimates of the Indonesian Throughflow entering the Indian Ocean: 2004–2006, Journal of Geophysical Research: Oceans, 114, 2009.

Stellema, A., Sen Gupta, A., and Taschetto, A. S.: Projected slow down of South Indian Ocean circulation, Scientific reports, 9, 1–15, 2019.

Stramma, L., Johnson, G. C., Sprintall, J., and Mohrholz, V.: Expanding oxygen-minimum zones in the tropical oceans, science, 320, 655–658, 2008.

750  Stramma, L., Prince, E. D., Schmidtko, S., Luo, J., Hoolihan, J. P., Visbeck, M., Wallace, D. W., Brandt, P., and Körtzinger, A.: Expansion of oxygen minimum zones may reduce available habitat for tropical pelagic fishes, Nature Climate Change, 2, 33–37, 2012.

Tachiiri, K., Abe, M., Hajima, T., Arakawa, O., Suzuki, T., Komuro, Y., Ogochi, K., Watanabe, M., Yamamoto, A., Tatebe, H., Noguchi, M. A., Ohgaito, R., Ito, A., Yamazaki, D., Ito, A., Takata, K., Watanabe, S., and Kawamiya, M.: MIROC MIROC-ES2L model output prepared for CMIP6 ScenarioMIP, https://doi.org/10.22033/ESGF/CMIP6.936, 2019.

755  Takano, Y., Ito, T., and Deutsch, C.: Projected centennial oxygen trends and their attribution to distinct ocean climate forcings, Global Biogeochemical Cycles, 32, 1329–1349, 2018.

Talley, L. D.: Descriptive physical oceanography: an introduction, Academic press, 2011.

Tang, Y., Rumbold, S., Ellis, R., Kelley, D., Mulcahy, J., Sellar, A., Walton, J., and Jones, C.: MOHC UKESM1.0-LL model output prepared for CMIP6 CMIP, https://doi.org/10.22033/ESGF/CMIP6.1569, 2019.

760  Tomczak, M. and Large, D. G.: Optimum multiparameter analysis of mixing in the thermocline of the eastern Indian Ocean, Journal of Geophysical Research: Oceans, 94, 16 141–16 149, 1989.

Vaquer-Sunyer, R. and Duarte, C. M.: Thresholds of hypoxia for marine biodiversity, Proceedings of the National Academy of Sciences, 105, 15 452–15 457, 2008.

Wieners, K.-H., Giorgetta, M., Jungclaus, J., Reick, C., Esch, M., Bittner, M., Gayler, V., Haak, H., de Vrese, P., Raddatz, T., Mauritsen, T.,
765  von Storch, J.-S., Behrens, J., Brovkin, V., Claussen, M., Crueger, T., Fast, I., Fiedler, S., Hagemann, S., Hohenegger, C., Jahns, T., Kloster, S., Kinne, S., Lasslop, G., Kornblueh, L., Marotzke, J., Matei, D., Meraner, K., Mikolajewicz, U., Modali, K., Müller, W., Nabel, J., Notz, D., Peters, K., Pincus, R., Pohlmann, H., Pongratz, J., Rast, S., Schmidt, H., Schnur, R., Schulzweida, U., Six, K., Stevens, B., Voigt, A., and Roeckner, E.: MPI-M MPIESM1.2-LR model output prepared for CMIP6 ScenarioMIP, https://doi.org/10.22033/ESGF/CMIP6.793, 2019a.

770  Wieners, K.-H., Giorgetta, M., Jungclaus, J., Reick, C., Esch, M., Bittner, M., Legutke, S., Schupfner, M., Wachsmann, F., Gayler, V., Haak, H., de Vrese, P., Raddatz, T., Mauritsen, T., von Storch, J.-S., Behrens, J., Brovkin, V., Claussen, M., Crueger, T., Fast, I., Fiedler, S., Hagemann, S., Hohenegger, C., Jahns, T., Kloster, S., Kinne, S., Lasslop, G., Kornblueh, L., Marotzke, J., Matei, D., Meraner, K., Mikolajewicz, U., Modali, K., Müller, W., Nabel, J., Notz, D., Peters, K., Pincus, R., Pohlmann, H., Pongratz, J., Rast, S., Schmidt, H., Schnur, R., Schulzweida, U., Six, K., Stevens, B., Voigt, A., and Roeckner, E.: MPI-M MPIESM1.2-LR model output prepared for CMIP6
775  CMIP, https://doi.org/10.22033/ESGF/CMIP6.742, 2019b.

Zhuang, J., Dussin, R., Huard, D., Bourgault, P., Banihirwe, A., Hamman, J., Jüling, A., Filipe, Rondeau, G., Rasp, S., and et al.: pangeo-data/xESMF: v0.5.2, https://doi.org/10.5281/zenodo.4464833, 2021.